Paleoceanography and Paleoclimatology

RESEARCH ARTICLE
10.1029/2018PA003391

Special Section:
Climatic and Biotic Events of the Paleogene: Earth Systems and Planetary Boundaries in a Greenhouse World

Warm Terrestrial Subtropics During the Paleocene and Eocene: Carbonate Clumped Isotope (Δ_{47}) Evidence From the Tornillo Basin, Texas (USA)

Julia R. Kelson[1], Dylana Watford[2], Clement Bataille[3], Katharine W. Huntington[1], Ethan Hyland[4], and Gabriel J. Bowen[2]

[1]Department of Earth and Space Sciences and Quaternary Research Center, University of Washington, Seattle, WA, USA, [2]Department of Geology and Geophysics, University of Utah, Salt Lake City, UT, USA, [3]Department of Earth and Environmental Sciences, University of Ottawa, Ottawa, ON, Canada, [4]Department of Marine, Earth, and Atmospheric Sciences, NC State University, Raleigh, NC, USA

Abstract Records of subtropical climate on land from the early Paleogene offer insights into how the Earth system responds to greenhouse climate conditions. Fluvial and floodplain deposits of the Tornillo Basin (Big Bend National Park, Texas, USA) preserve a record of environmental and climatic change of the Paleocene and the early Eocene. We report carbon, oxygen, and clumped isotopic compositions ($\delta^{13}C$, $\delta^{18}O$, and Δ_{47}) of paleosol carbonate nodules from this basin. Mineralogical, geochemical, and thermal modeling evidence suggests that the measured isotopic values preserve primary environmental signals with a summer bias with the exception of data from two nodules reset by local igneous intrusions. The unaltered nodules record Δ_{47} temperatures of 25 ± 4 and 32 ± 2 °C for the Paleocene and early Eocene nodules, respectively, showing an increase in average summer temperatures of 7 ± 3 °C. Calculations of $\delta^{18}O$ of soil water are −2.8 ± 0.7‰ and −0.8 ± 0.4‰ (standard mean ocean water) for the early-mid-Paleocene and late Paleocene-early Eocene, showing an increase of 2.0 ± 0.9‰. The increase in temperature and $\delta^{18}O$ values likely relates to a rise in atmospheric pCO_2, although we cannot rule out that changes in paleosol texture and regional precipitation patterns also influence the record. Comparison with Δ_{47} estimates of summer temperature from the Green River and Bighorn Basins (WY) highlights that terrestrial surface temperatures are heterogeneous, and latitudinal temperature gradients on land remain undetermined. Previously published paleoclimate models predict summer temperatures that are 2 to 6 °C higher than our estimate; discrepancies between climate models and proxy data persist at lower latitudes.

Key Points:
- Paleosol carbonate nodules from the Tornillo Basin record primary environmental values of carbon, oxygen, and clumped isotopes
- Carbonate nodules record average clumped isotope temperatures of 25 ± 4 and 32 ± 2 °C for the Paleocene and early Eocene, respectively
- These temperature estimates are lower than model predictions, and data-model discrepancies remain at low latitudes for the Eocene

Supporting Information:
- Supporting Information S1
- Table S1
- Table S2
- Table S3
- Table S4

Correspondence to:
J. R. Kelson,
jrkelson@uw.edu

Citation:
Kelson, J. R., Watford, D., Bataille, C., Huntington, K. W., Hyland, E., & Bowen, G. J. (2018). Warm terrestrial subtropics during the Paleocene and Eocene: Carbonate clumped isotope (Δ_{47}) evidence from the Tornillo Basin, Texas (USA). *Paleoceanography and Paleoclimatology*, *33*. https://doi.org/10.1029/2018PA003391

Received 18 APR 2018
Accepted 8 OCT 2018
Accepted article online 11 OCT 2018

1. Introduction

Reconstructions of ancient greenhouse climates can help inform our understanding of future climates that could be similarly forced by high concentrations of atmospheric CO_2. Greenhouse climates of the early Paleogene provide examples of Earth's long-term sensitivity of climate to high CO_2 (Haywood et al., 2011; Lunt et al., 2012, 2013; Valdes, 2011); the early Paleogene contains peak global temperatures of the Cenozoic during the early Eocene climatic optimum (EECO; ~52 to 50 Ma), and those maximum temperatures correspond with high concentrations of atmospheric CO_2 (Anagnostou et al., 2016; Beerling & Royer, 2011; Hyland & Sheldon, 2013; Jagniecki et al., 2015; Lowenstein & Demicco, 2006; Pagani et al., 2005; Pearson et al., 2007; Zachos et al., 2008). Continuous records of ocean temperature exist from the Paleogene (Lauretano et al., 2015; Thomas et al., 2011; Zachos et al., 2001, 2008), but few terrestrial records span the entirety of the Paleocene and the transition into the early Eocene. The need for proxy estimates of temperature on land during this past greenhouse period is highlighted by predictions that terrestrial warming can outpace oceanic warming (Diffenbaugh & Field, 2013).

Fundamental questions about the nature and dynamics of early Paleogene climates remain unanswered. In particular, latitudinal temperature gradients in the early Eocene are enigmatic because shallow gradients estimated by proxies are challenging to reproduce with climate models (Bernard et al., 2017; Heinemann et al., 2009; Ho & Laepple, 2016; Huber & Caballero, 2011; Lunt et al., 2012, 2016; Matthew & Sloan, 2001; Roberts et al., 2009; Sagoo et al., 2013; Sewall & Sloan, 2006, 2001; Shellito et al., 2003, 2009; Sloan, 1994; Sloan & Barron, 1990; Thrasher & Sloan, 2009; Tierney et al., 2017; Winguth et al., 2010). Both geochemical

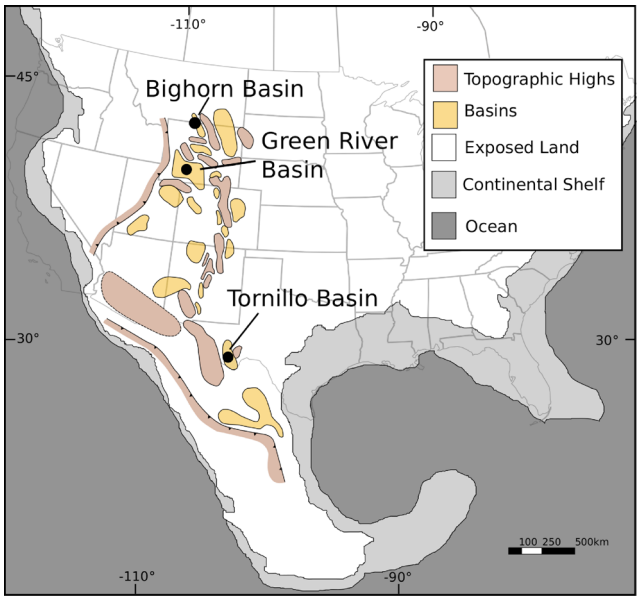

Figure 1. Location of the Tornillo Basin (Big Bend National Park), Texas, in relation to other Laramide Basins, the proto-Gulf of Mexico, and modern states. Map modified from Galloway et al. (2011).

proxies and fossils generally predict early Paleogene high-latitude temperatures that are much higher than modern, often by 20° or more (Brinkhuis et al., 2006; Eberle et al., 2010; Eberle & Greenwood, 2012; Greenwood & Wing, 1995; Hollis et al., 2009; Maxbauer et al., 2014; Pross et al., 2012; Royer et al., 2002; Sluijs et al., 2008, 2009, 2006; Smith et al., 2009; Spicer & Parrish, 1990; Weijers et al., 2007). Global climate models have been able to reproduce this high latitude warmth with large radiative forcing (Huber & Caballero, 2011; Lunt et al., 2012). However, these models also predict extremely high temperatures at low latitudes that, in some cases, exceed the physiological temperature limit for plant and animal survival (Huber, 2008; Sherwood & Huber, 2010). They are thus difficult to reconcile with fossil records that suggest mild tropical climates and/or abundant tropical life (Head et al., 2009; Spicer et al., 2014; Wheeler & Lehman, 2005; S. Wing & Greenwood, 1993; S. L. Wing et al., 2005, 2009) and disagree with some geochemical proxy reconstructions of mild tropical climates (Bijl et al., 2009; Evans et al., 2018; Keating-Bitonti et al., 2011). However, other studies voice concerns about the accuracy and interpretation of some geochemical ($\delta^{18}O$ and TEX_{86}) proxy reconstructions of low-latitude Paleogene climate due to problematic calibrations and/or sample preservation (Aze et al., 2014; Frieling et al., 2017; Hollis et al., 2012; Kozdon et al., 2011; Pearson et al., 2001, 2007). Furthermore, some fossil records provide evidence for heat-stressed organisms and hot tropical temperatures that are more consistent with model predictions (Frieling et al., 2017; Harrington & Jaramillo, 2007; Head et al., 2009; Jaramillo et al., 2006). Additional quantitative proxy estimates of subtropical temperatures on land during greenhouse periods such as the early Paleogene offer a crucial opportunity to test model predictions and expand the representation of low-latitude temperatures in proxy data sets.

Early Paleogene warming was also accompanied by global hydrologic changes that remain poorly understood and likely varied with geography and with the temporal scale of interest (Anhäuser et al., 2018; Carmichael et al., 2015, 2016, 2017; Foreman et al., 2012; Kraus et al., 2015; Kraus & Riggins, 2007; McInerney & Wing, 2011; Schmitz & Pujalte, 2007; Smith et al., 2014). It has been hypothesized that increased warming during greenhouse periods is associated with a more intense hydrologic cycle (e.g., Held & Soden, 2006), which could be manifested partly as increased summertime precipitation in North America (Huber & Goldner, 2012; Schubert et al., 2012; Sewall & Sloan, 2006; Thrasher & Sloan, 2009). Improved understanding of patterns of hydroclimate in the early Paleogene would offer potential to test this prediction and document specific characteristics of the water cycle of greenhouse climates.

Here we expand our understanding of subtropical terrestrial temperatures and hydrology during the Paleocene and the early Eocene by applying the carbonate clumped isotope paleothermometer (Δ_{47}) to a suite of paleosols in the Tornillo Basin in Big Bend National Park, Texas (Figure 1). The paleosol sequence in the Tornillo Basin preserves a long, well-sampled record of environmental change from the early Paleocene through early Eocene (Atchley et al., 2004; Bataille et al., 2016, 2018). Carbonate clumped isotopes can provide information on both soil temperatures and meteoric waters at the time of carbonate growth, which allows us to provide a quantitative estimate of terrestrial environmental changes across this important greenhouse interval in the previously undersampled subtropics.

2. Materials and Methods

2.1. Paleogeographic, Geologic, and Environmental Setting

The paleosols studied in this work are from the Tornillo Basin in Big Bend National Park, Texas (USA), approximately 29°25′N, 103°09′W (Figure 1). The Tornillo Basin formed as the southernmost extent of the Laramide orogeny (Lehman, 1991; Lehman & Busbey, 2007; Lehman et al., 2018; Schiebout et al., 1987; Turner et al., 2011) and during the early Paleogene was likely at or near the same subtropical latitude as it is today (van Hinsbergen et al., 2015). There is some evidence for syndepositional deformation in the studied

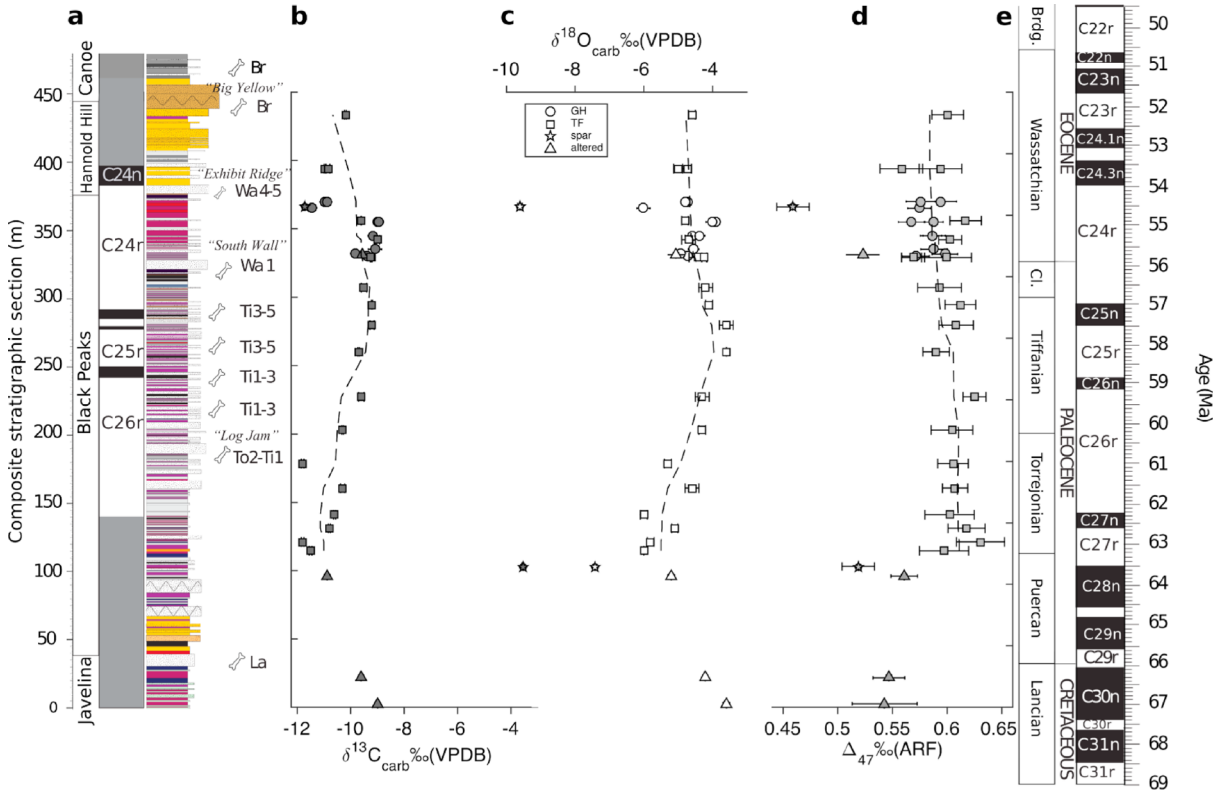

Figure 2. Stratigraphy, age model, and isotopic composition of carbonate nodules from the Tornillo Group (modified from Bataille et al., 2016, 2018). (a) Composite stratigraphy from Tornillo Flats and Grapevine Hills. Magnetostratigraphic and biostratigraphic data are linked to the composite section (Rapp et al., 1983; Schiebout et al., 1987). The gray shading in the magnetostratigraphic data is the unstudied intervals. (b–d) Symbols indicate sampling section (GH = Grapevine Hills, TF = Tornillo Flats), and star and triangle symbols are either spar or diagenetically altered samples, as discussed in section 4.1. Errors for $\delta^{13}C$ and $\delta^{18}O$ are standard deviation and are generally smaller than the symbols. Errors for Δ_{47} are standard error. Dashed lines are a moving average of the isotopic data, excluding the spar and altered samples. (e) Timescale with geologic epochs and ages, global magnetic polarity zones, and North American Land Mammal Ages.

Paleocene and Eocene sediments (Lehman & Busbey, 2007). The basin was likely a distal foreland basin with relatively low sediment accumulation rates (Schiebout et al., 1987). During the Paleogene, the basin was close to the proto-Gulf of Mexico shoreline and thus preserves a record of a more coastal environment than exists at modern Big Bend (e.g., Galloway et al., 2011; Sharman et al., 2017).

We focus on Paleocene to early Eocene sediments in the Black Peaks and Hannold Hill Formations (Figures 1 and S2 in the supporting information). These sediments consist of alternating channel deposits and overbank floodplain deposits with evidence of pedogenesis (Bataille et al., 2016; Lehman & Busbey, 2007; White & Schiebout, 2008). Identifiable paleosols have been measured and described from these sections (Figures 2 and S1), and some of the pedogenic horizons yield carbonate nodules. An age model for these sediments was developed using carbon isotope stratigraphy, magnetostratigraphy, and sparse vertebrate fossils (Bataille et al., 2016, 2018; Rapp et al., 1983; Schiebout et al., 1987) and agrees well with a paleomagnetically constrained age model for a section with overlapping stratigraphic coverage that is exposed about 38 km to the west (Leslie et al., 2018).

2.2. Field Methods

Stratigraphic sections were measured in two adjacent locations exposing the target formations, at Tornillo Flats and at Grapevine Hills (Figures 2, S1, and S2). Sections were correlated primarily via two distinct marker beds: the Exhibit Ridge sandstone and the uppermost black paleosol of the Black Peaks Fm. Between these marker beds, sections were correlated based on similar lithologies and thicknesses and measurements of dip (Bataille et al., 2016; Figure S1). Paleosols were identified in the field based on pedogenic features such as horizonation, coloring, root traces and burrowing, gleying, and/or the presence of carbonate nodules.

Paleosols were trenched to enable accurate description, and samples were collected from at least 20 cm below the modern outcrop surface to avoid modern contamination and exposure weathering. Carbonate nodules were sampled from the middle of the Bk horizon. The depth to the Bk horizon ranged from 0.1 to 4 m below the approximate top of the paleosol horizon; however, there is significant uncertainty in this estimate because the tops of most paleosols were either truncated or indistinct due to continual aggradation and pedogenesis. The shallowest of these carbonates (~0.1 m) were collected from truncated paleosols and the true formation depth is unknown. We collected bulk A and B horizon materials and pedogenic carbonate nodules where present.

2.3. Carbonate Analysis Methods

2.3.1. Nodule Characterization and Sampling

Each carbonate nodule was cut open and polished for examination and selected carbonate nodules were made into thin sections. The carbonate nodules from Tornillo Flats were prepared and described as part of an MS thesis (Watford, 2015), and five of those nodules had thin sections that were examined with transmitted light. We collected additional nodules from Grapevine Hills, and representative nodules from that section were made into thin sections that were examined with both transmitted light and cathodoluminescent (CL) microscopy. The CL scope used is a Luminoscope ELM-3R and was operated at 5–10 kV, 0.5 mA, and 50–100 mTorr. Nodules were classified as homogeneous, heterogeneous, or radial, based on their internal textures, where homogeneous nodules were dominated by homogeneous micritic carbonate, heterogeneous nodules showed appreciable brecciation, grainification, and/or phreatic sparry calcite cement, and radial nodules exhibited a distinctive radial-fibrous fabric (example images in Watford, 2015, and Bataille et al., 2016). With one exception, radial nodules were not analyzed for Δ_{47} given previous work suggesting that they represented distinctive, groundwater-dominated growth environments characterized by unusual isotopic values (Bataille et al., 2016; Schmidt, 2009). For all nodules, the target carbonate material was sampled from the cut and polished nodule surface using a micromill, a mounted dental drill, or by hand with a drill tool. One nodule was too small to be cut open ($<$0.5 cm in diameter), so the entire nodule was ground and homogenized (PS3); this sampling method offers considerably more opportunity for unintentional sampling of altered material.

2.3.2. $\delta^{18}O$, $\delta^{13}C$, and Δ_{47} Methods

Soil carbonates grow in near-equilibrium conditions (Quade, Garzione, et al., 2007; Quade et al., 2013) and thus can provide a reliable record of growth temperature and isotopic composition of the source fluid and gases. Carbonate clumped isotope thermometry uses the thermodynamic preference for an increase in the abundance of ^{13}C-^{18}O bonds with decreasing temperature in order to measure the growth temperature of a carbonate mineral (e.g., Affek, 2012; Eiler, 2007; Ghosh et al., 2006). Paired with the simultaneously measured oxygen isotope ($\delta^{18}O$) composition of carbonate, the $T\Delta_{47}$ also allows for the calculation of the $\delta^{18}O$ of the water in which the carbonate grew (here denoted $\delta^{18}O_w$; e.g., Eiler, 2011; Huntington & Lechler, 2015; Quade et al., 2013).

The $\delta^{18}O$, $\delta^{13}C$, and Δ_{47} compositions of the carbonate nodules were measured at the University of Washington IsoLab in Seattle, WA. First, 6–10-mg carbonate-equivalent of sample powder was digested in a common bath of phosphoric acid with a specific gravity of 1.904–1.970 g/cm^3 held at 90 °C. We do not observe a change in measured Δ_{47} in our carbonate standards across this range in specific gravity. The evolved CO_2 gas was then cryogenically purified using an offline, automated vacuum system. The purified CO_2 gas was measured on a Thermo MAT 253 mass spectrometer configured to measure *m/z* 44–49. Details of the purification and the measurements, including the pressure baseline, absolute reference frame, and ^{17}O correction are described elsewhere (Burgener et al., 2016; Kelson et al., 2017; Schauer et al., 2016). For every approx. four sample unknowns, a carbonate standard was run, which rotated between a tropical Porites coral (Coral), two in-house reagent-grade synthetic carbonates (C64 and C2), and four synthetic carbonates distributed by ETH Zurich (ETH1–4; Bernasconi et al., 2018; Meckler et al., 2014). We regularly purified and measured heated gases (1,000 °C) and equilibrated gases (4 and 60 °C) to place samples into the absolute reference frame (Dennis et al., 2011). The sample analyses span four reference frames: a reference frame from February to October 2014, a reference frame from October 2014 to April 2015, a reference frame from October 2015 to December 2016, and a reference frame from December 2016 to April 2018.

Δ_{47} was calculated using standard methods (Dennis et al., 2011; Huntington et al., 2009), with two exceptions: we used the Brand et al. (2010) parameters to correct for ^{17}O interference (Daëron et al., 2016; Schauer et al., 2016), and we did not add an acid fractionation factor to our Δ_{47} values (values are presented in the 90 °C reference frame). Each nodule was analyzed in replicate two to eight times (replication is defined as an individual acid digestion of a subset of the sample powder). We calculated temperatures from Δ_{47} values ($T\Delta_{47}$) with the calibration presented in Kelson et al. (2017, equation 2), which is similar to other recent clumped isotope calibrations (e.g., Bonifacie et al., 2017), and was produced at IsoLab with the same methods (also calculated with the Brand et al., 2010, parameters and used carbonates digested in 90 °C acid). We report two estimates of error: (1) standard error (S.E.), which was calculated as the larger of either the standard deviation of the sample Δ_{47} or our external error of 0.021‰ (estimated by the long-term standard deviation of our zeros), divided by the square root of the number of replicates for that sample; and (2) the 95% confidence interval (CI), which was calculated as the Student's *t* value for the number of replicates multiplied by the S.E. Although errors on individual samples can be quite large, robust estimates for temperature can be made by using an error-weighted average of samples from similar time periods and reporting the 95% CI on those means (Fernandez et al., 2017). The $\delta^{18}O$ composition of the fluids from which the carbonates grew ($\delta^{18}O_w$) was estimated using the $T\Delta_{47}$ and the calcite-water fractionation factors from Kim and O'Neil (1997). The error in the $T\Delta_{47}$ measurement was propagated to estimate the error in the $\delta^{18}O_w$ calculation.

3. Results

3.1. Carbonate Nodule Texture Observations

Most of the carbonate nodules (>70%) were characterized as homogenous, and micritic material from those nodules was targeted for isotopic analysis. Examination of thin sections in plane light showed that some of the homogenous nodules contained some secondary spar (>10 μm). The spar was isolated to veins or inclusions and made up less than 10% of the total nodule, which enabled us to sample exclusively micrite for isotopic analysis. In two nodules (BB-TF2-14-036 and BB-TF3-14-003), we were able to isolate and sample the spar material for isotopic analysis (Table S1). Thin section imagery revealed that the sparry calcite exhibited red or orange luminescence that was distinct from the micritic material, which was uniformly nonluminescent (Figure S3). The minor amount of spar, together with textural observations from CL, suggests that examination in plane light was likely sufficient to allow sampling for isotopic analyses that avoided most secondary or diagenetic calcite material.

3.2. $\delta^{18}Oc$, $\delta^{13}C$, Δ_{47}, and $\delta^{18}O_w$ Results

Micritic carbonate samples have $\delta^{18}O_c$ values that range from −3.6‰ to −10.1‰ (Vienna Pee Dee belemnite (VPDB)) with an average S.E. of 0.04‰ and $\delta^{13}C$ values that range from −8.9‰ to −11.8‰ (VPDB) with an average S.E. of 0.09‰. Mean Δ_{47} values of the micritic carbonate nodules range from 0.456% to 0.646‰, with S.E. that ranges from 0.009% to 0.029‰ (Table S1, Figure 2). This corresponds to $T\Delta_{47}$ values that range from 13 to 89 °C with 95% CI that ranges from 7 to 47 °C. Using the $\delta^{18}O_c$ and $T\Delta_{47}$ from individual carbonate nodules, we calculate a range in $\delta^{18}O_w$ of −5.8‰ to 3.0‰ (Vienna standard mean ocean water (VSMOW)) with error ranging from 0.5‰ to 1.5‰ (Table S1 in the supporting information and Figures 4 and 5).

4. Discussion

4.1. Recognizing Diagenesis

Postdepositional alteration can destroy the primary climate signal in a pedogenic carbonate nodule. Alteration can occur either through secondary precipitation of calcite or through solid-state reordering of the ^{13}C-^{18}O bonds. Recrystallization or precipitation of secondary calcite can cause the Δ_{47}, and conditionally also the $\delta^{13}C$ and $\delta^{18}O$, values of carbonate nodules to reflect the temperature and isotopic composition of the secondary fluid. Solid-state reordering can occur if a carbonate mineral is held at temperatures of >100 °C for an extended amount of time (>10^6 years), thus changing Δ_{47} but not $\delta^{18}O$ or $\delta^{13}C$ of carbonate (Henkes et al., 2014; Lloyd et al., 2017; Passey & Henkes, 2012; Stolper & Eiler, 2015). Here we discuss the possibility that these two processes have altered the Big Bend carbonate nodules.

4.1.1. Spar Indicates Localized Recrystallization

In Big Bend, fluids associated with late Eocene-early Oligocene magmatic intrusions could have recrystallized the carbonate nodules. Thin sections of the nodules reveal distinct accumulations of luminescent spar (Figure S3), which can be explained by increased concentrations in trace metals that are associated with secondary precipitation (e.g., Finnegan et al., 2011). Indeed, our two measured spar samples have $T\Delta_{47}$, $\delta^{13}C$, and $\delta^{18}O$ compositions that are distinctly higher than those of micrite samples (Table S1). The range in bulk isotopic composition among these samples (~10‰ in both $\delta^{13}C$ and $\delta^{18}O$) might be due to multiple phases of recrystallization with fluids varying in composition. We carefully sampled carbonate nodules where possible in order to avoid contamination from diagenetic spar material and believe that our isotopic analyses of micrite are not significantly contaminated with recrystallized postburial phases.

4.1.2. Potential Solid-State Reordering of Micritic Samples Due to Heating From Burial and Local Laccoliths

Solid-state reordering does not necessarily change the visible texture or bulk elemental structure of carbonates, which makes it nearly impossible to observe from thin-section imagery alone. Here we use thermal modeling to explore the possibility that our sample carbonate nodules could have experienced partial or complete reordering.

It is unlikely that the sampled sediments reached burial temperatures higher than 100 °C because they were never deeply buried (also assumed by Atchley et al., 2004; Nordt et al., 2011; heating due to local volcanic deposits is considered later). The combined Black Peaks, Hannold Hill, and Canoe Formations are approximately 720–820-m thick (Turner et al., 2011). The Chisos Formation (~1,000 m thick) is time-correlative with the Canoe Formation, but its distribution is limited to a local basin southwest of the stratigraphic sections measured, and thus, it does not overlie the sediments of interest (Turner et al., 2011). No other potential Paleogene overburden is mapped in this area. There are late Tertiary to Quaternary alluvial sediments in the region, but their deposition is localized in fault-bounded basins, and any such alluvial accumulation in the vicinity of Tornillo Flats and Grapevine Hills likely had an insignificant effect on burial temperatures of the study formations (Turner et al., 2011). Therefore, the sediments of the Black Peaks and Hannold Hill Formations were buried <1 km, and so a remarkably high geothermal gradient would have been required to heat the carbonates studied here to >100 °C. Even if late Tertiary Basin and Range extension elevated the geothermal gradient in the region to a high gradient like that of continental magmatic arc regions, ~40 to 50 °C/km (Rothstein & Manning, 2003), the sediments would have been buried at maximum temperatures of 60–70 °C. Heating of temperatures <100 °C could have promoted modest reordering (an increase in apparent temperature of 10 °C) if the carbonate samples resided at those elevated temperatures for hundreds of millions of years (Stolper & Eiler, 2015), but these samples have a maximum depositional age of 70 Ma that rules out such a long burial history. Thus, heating due to burial alone is unlikely to have significantly altered the clumped isotope bonding in our carbonate nodules.

Several kilometer-scale laccoliths were emplaced in the region at ~32 Ma (Miggins et al., 2007) and could have provided enough heat to locally enable solid-state reordering. The Grapevine Hills section is so-named due to the Grapevine Laccolith that is as close as 0.8 km to our stratigraphic section (Figure S2). Geophysical measurements of the Grapevine Laccolith suggest that it is about 3.5 km wide and 200 m thick and that the laccolith does not extend laterally beyond its surface expression (Turner et al., 2011). We model the heating of the country rock using the 1D error function solution to the Fourier conduction equation (e.g., Turcotte & Schubert, 2014). We model the laccolith as a body of basaltic composition that is 200 m thick with a starting temperature of 1,400 °C (this starting temperature includes an adjustment for the latent heat of crystallization; e.g., Philpotts, 1990) and a thermal diffusivity of $1e^{-6}$ m^2/s. At a distance of 800 m from the laccolith (our closest sampling location), the country rock reaches simulated temperatures of up to 113 °C for ~2 Ma (Figures 3a and 3b). This estimate is inherently an overestimate of the heat at this sampling location because we model heat conduction in only one dimension, and in reality, heat can diffuse into the country rock in several directions. Also, the sample is located off of the edge of the laccolith, so the sample location would experience lower maximum temperatures. The relatively low temperatures predicted by our thermal modeling are consistent with the absence of evidence for contact metamorphism in sediments and paleosols surrounding the laccolith at Grapevine Hills (i.e., no color or textural changes). Given this thermal history, the Passey and Henkes (2012) model for reordering of clumped isotopes in carbonate predicts an increase in apparent clumped isotope temperature of <1 °C using the Arrhenius parameters from a brachiopod

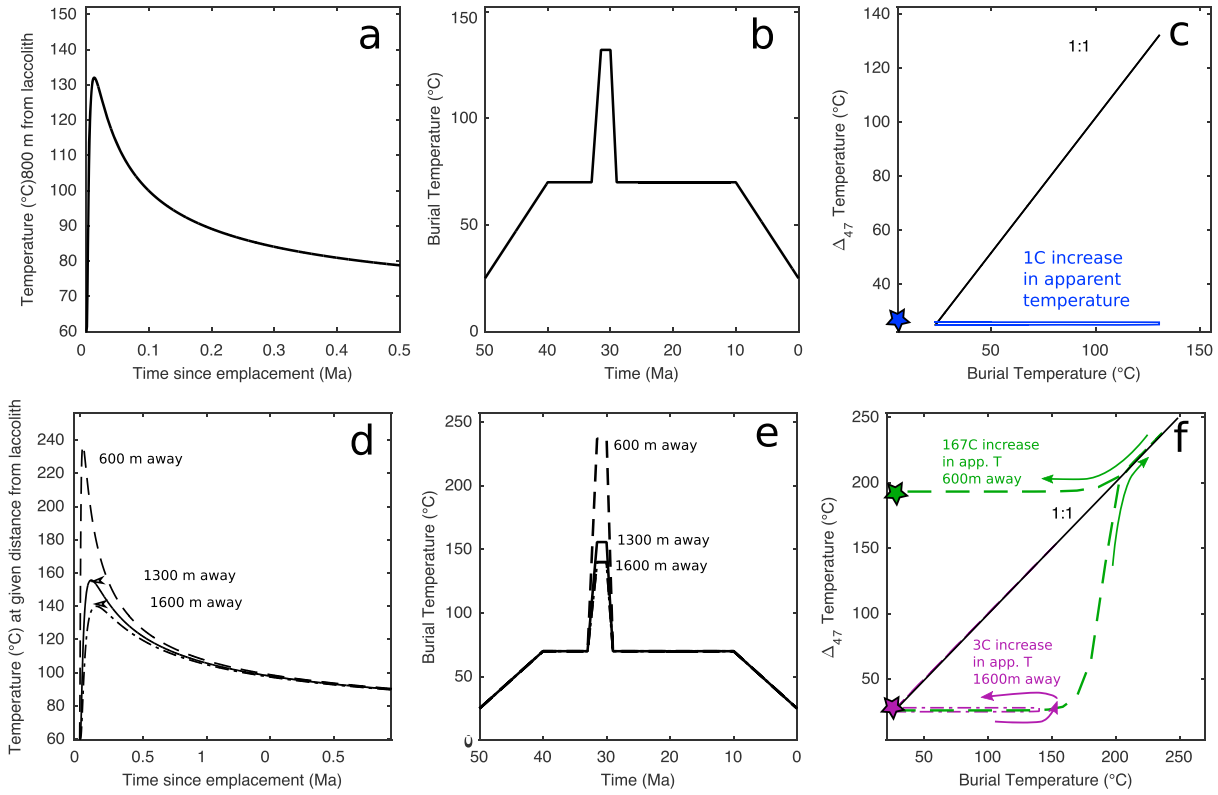

Figure 3. Thermal history of the two sample locales, Grapevine Hills (a–c) and Tornillo Flats (d–f). (a) For a laccolith that is 200 m thick, a 1D equation for heat diffusion predicts that a location 0.8 km away from the laccolith edge would reach ~130 °C, then cool to temperatures less than 100 °C by <0.1 Ma. (b) An approximate thermal history of the basin, where sediments start at 35 °C on the surface, are buried to 70 °C, are heated by a laccolith at 33 Ma to 113 °C for 2 Ma, are cooled to 70 °C, and then are rapidly exhumed to the surface starting at 10 Ma. Apparent $T\Delta_{47}$ calculations are not sensitive to temperatures <100 °C, so details of the thermal history below that temperature are not important. (c) The solid-state reordering model of Henkes et al. (2014) predicts an increase of <1 °C in the apparent $T\Delta_{47}$. The black line is a 1:1 line. The blue line is the temperature path for the carbonate. The blue star indicates the final apparent temperature. (d) For a laccolith that is 450 m thick, we show predictions for temperatures experienced at 600, 1,300, and 1600 m away from the laccolith. (e) Thermal histories for the sediments at those distances from the laccolith, where sediments start at 25 °C on the surface, are buried to 70 °C, are heated by a laccolith at 33 Ma, are cooled to 70 °C, and then are exhumed to the surface starting at 10 Ma. (f) Reordering calculations at distances of 600 and 1,600 m in green and purple, respectively (1,300 m omitted for clarity), and the colored stars indicate the final apparent temperature.

(WA-CB-13), a result which is not sensitive to the assumed starting $T\Delta_{47}$ (Figure 3c). This increase in temperature is too small to resolve with current Δ_{47} precision. In conclusion, it is unlikely that the Grapevine Laccolith provided enough heat to promote measurable solid-state reordering of the clumped isotope bonds in our sampled carbonates.

The Rosillos Laccolith north of Tornillo Flats should also be considered as a heat source that could enable solid state reordering in nearby samples. The Rosillos Laccolith is 600 m thick on its north end, thinning to 200 m on its south end (Turner et al., 2011). The two Cretaceous Javelina Formation samples collected in northern Tornillo Flats are as close as 1 km to the south end of the laccolith (Figure S2). We model the Rosillos Laccolith conservatively as 450 m thick, with the same temperature and thermal diffusivity as above. Using the Passey and Henkes (2012) reordering model and a starting sample depositional temperature of 25 °C, we predict an apparent $T\Delta_{47}$ of 28 °C at a distance of 1.6 km, an apparent $T\Delta_{47}$ of 50 °C at a distance of 1.3 km, and an apparent $T\Delta_{47}$ of 192 °C at a distance of 0.6 km (Figures 3d, 3e, and 3f). Note that these predicted temperatures imply that partial resetting could occur depending on the proximity to the intrusion; the apparent temperature predicted is less than the maximum temperature the sample at that distance experiences. Again, these are likely overestimates of the effect of heating because we have modeled the heat diffusion in only one direction and the samples are at the edge of the laccolith where the heat is able to diffuse in multiple directions. The carbonate nodules that are <1.3 km away from the Rosillos Laccolith have relatively high measured $T\Delta_{47}$: BB-TF2-14-002 has a temperature of 49 ± 32 °C, and BB12–077 has a temperature of

47 ± 11 °C. These measurements are consistent with modeled temperature effects, and so we interpret these high temperatures as potentially indicating that these samples experienced solid-state reordering when the Rosillos Laccolith was emplaced. Therefore, we exclude these two samples from our environmental interpretations but maintain that all other measured samples are unlikely to have experienced solid-state reordering.

4.1.3. Problematic Carbonate Nodules

Carbonate nodule PS3 was too small (~2 mm in diameter) to make a thin section or microsample, so the entire nodule was ground up and analyzed. If secondary carbonate phases were present in this nodule, they would have been included in our clumped isotope sample and may have affected the resulting data. Indeed, this nodule has a clumped isotope temperature that is hotter than plausible Earth surface temperatures ($T > 55$ °C) but consistent with a mixture of spar and micrite. We exclude this carbonate nodule from our paleoclimate reconstruction.

The only carbonate nodule sampled from a black paleosol (BB-TF2-14-030) exhibited a radial fabric and has a relatively high clumped isotope temperature (48 ± 14 °C). Carbonate nodules from black paleosols in this formation were previously excluded from $\delta^{13}C$ chemostratigraphy because these paleosols indicate carbonate growth in a water-saturated environment where the carbonates might incorporate a higher contribution of carbon from respired soil CO_2 compared to carbonate nodules from other soils in the section (Bataille et al., 2016; Mintz et al., 2011). The carbonate growth process is poorly understood in Histosol-like soils such as the black paleosols in the Black Peaks Formation and could involve disequilibrium processes, so we also exclude this nodule from our climate reconstruction.

4.2. Increase in Temperatures From the Paleocene to the Eocene

The most robust conclusions about climate arise from averaging multiple Δ_{47} analyses of multiple carbonate nodules; uncertainty in clumped isotope measurements prevents robust conclusions to be drawn from three to five analyses of a single carbonate sample (e.g., Fernandez et al., 2017). Thus, we only interpret the average temperatures of the multiple carbonate nodules that can be calculated by separating the record at the Paleocene-Eocene boundary. We choose this boundary because it is known to be of geologic significance (e.g., McInerney & Wing, 2011). Statistical evidence that supports treating the data as a constant piecewise function with a breakpoint at ~56 Ma can be found in the supporting information Text (S1) and Figure S4.

Our measurements show that on average the Eocene clumped isotope temperatures are higher than those from the Paleocene (32 ± 2 and 25 ± 3 °C, respectively; means are error weighted, and error is 95% CI of the mean; mean of all data is 28 ± 1.5 °C; Figure 4). A *t* test using the mean $T\Delta_{47}$ of each nodule finds that the Paleocene and Eocene have temperatures that are different by 7 ± 3 °C ($p = 0.025$). A *t* test using the individual Δ_{47} replicates confirms a statistically significant difference between the Paleocene and Eocene Δ_{47} values ($p = 0.0049$).

Although the Paleocene samples are dominantly from Tornillo Flats, and the Eocene samples are dominantly from Grapevine Hills, it is unlikely that the shift in temperatures between the Paleocene and Eocene could be explained only by differences between these closely situated localities. Bias due to the change in section sampled seems unlikely because the stratigraphy is similar between the two sections and they are less than 3 km apart. Furthermore, a *t* test suggests that there is no statistical difference between the Eocene-aged nodules from Tornillo Flats versus the nodules from Grapevine Hills ($p = 0.5027$). Additionally, if the samples from Grapevine Hills are removed and a *t* test for the Paleocene versus Eocene samples from Tornillo Flats is performed, the difference in temperature between the two periods of time is confirmed ($p = 0.0136$).

To interpret the significance of the temperature difference between the Paleocene and the Eocene, we must consider the seasonal bias of our proxy. Soil carbonate typically accumulates when an increase in soil temperature promotes soil matrix drying, and soil water reaches supersaturation with respect to carbonate (Breecker et al., 2009). This often occurs in summer months, and most studied modern soil carbonates with Δ_{47} data thus far record summer-biased temperatures (Burgener et al., 2016; Hough et al., 2014; Passey et al., 2010; Quade et al., 2013; Ringham et al., 2016). However, some soil carbonates record temperatures closer to mean annual temperature, likely due to differences in local precipitation and soil moisture regimes (Burgener et al., 2016; Gallagher & Sheldon, 2016; Peters et al., 2013). Thus, it is possible to hypothesize that the observed increase in temperature from the Paleocene to the Eocene could be related to an enhanced summer bias in the Eocene soils rather than a global increase in air temperatures.

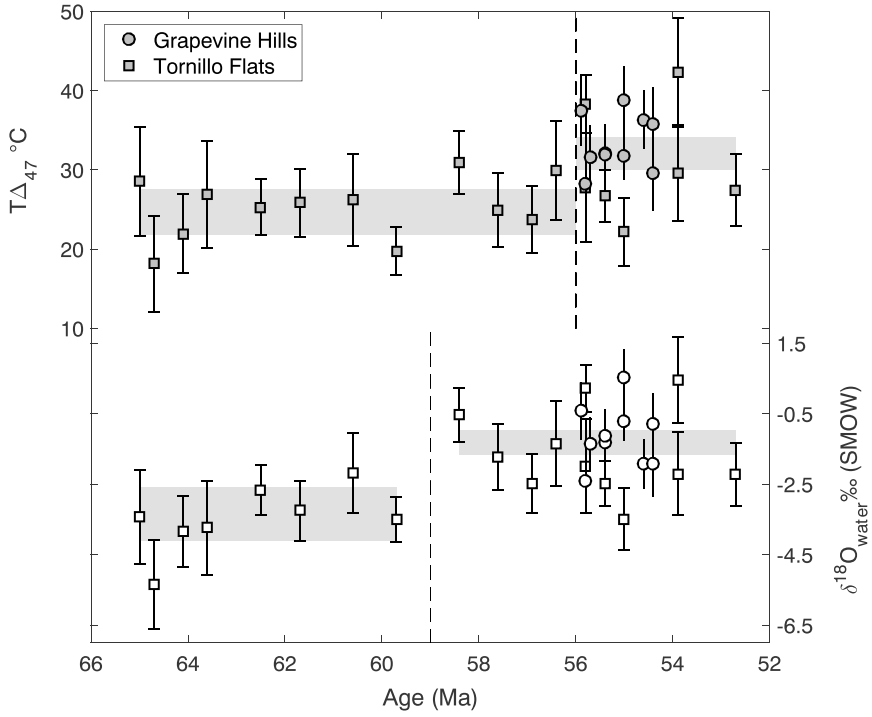

Figure 4. Calculated $T\Delta_{47}$ and $\delta^{18}O_w$ values for the carbonate nodules that record primary environmental values. Error bars on individual nodules in black are 1 standard error (the error normally reported for clumped isotope data). The vertical dashed line marks the point in time that minimizes root mean square misfit when modeling the data as two periods of time with a constant mean (56 Ma for $T\Delta_{47}$ and 59 Ma for $\delta^{18}O_w$). The gray rectangles are the 95% confidence interval centered on the error-weighted mean of the carbonate nodules for the given time period. SMOW = standard mean ocean water.

Sedimentological observations do suggest differences in precipitation and soil texture between the Paleocene and the early Eocene in Big Bend, but these factors are unlikely to lead to a shift in the seasonal bias of pedogenic carbonate accumulation that would fully explain temperature differences between these periods. The Paleocene environment in Big Bend was likely subtropical and humid with year-round precipitation (Wheeler, 1991): dark purple Alfisols alternating with black, Histosol-like horizons (Lehman, 1990) suggest the soils were relatively poorly drained. In these humid conditions, soil carbonate accumulation is most likely to occur during the summer because higher temperatures would increase the amount of soil water lost due to evaporation and uptake by plant roots. In the Eocene, climate models suggest precipitation in the region may have been more seasonal with stronger summer monsoon rainfall than the Paleocene (Carmichael et al., 2015; Sewall & Sloan, 2006; Thrasher & Sloan, 2009)—a shift that has also been inferred from the sandstone sedimentology in Big Bend (Bataille et al., 2018) and in the Green River Basin (Krueger, 2017). Some soils in strongly seasonal rainfall regimes experience delayed drying and record mean annual rather than summer temperatures (e.g., Peters et al., 2013). However, the Early Eocene soils at Big Bend were well drained (Bataille et al., 2016; White & Schiebout, 2008) and likely dried shortly after summer rain events (as observed by Breecker et al., 2009 and Ringham et al., 2016), resulting in a summer bias, as we infer for Paleocene carbonate accumulation. Therefore, it is unlikely that a change in the seasonal bias of the soil carbonates can explain the temperature difference we observe in the Paleocene and the Eocene samples.

The shift in temperatures at the start of the Eocene more likely relates to a contemporaneous gradual rise in the concentration of atmospheric pCO_2 (Anagnostou et al., 2016; Beerling & Royer, 2011; Cui & Schubert, 2017; Hyland & Sheldon, 2013; Jagniecki et al., 2015; Maxbauer et al., 2014; D. L. Royer et al., 2014). The increase in temperatures at Big Bend is also contemporaneous with an increase in $\delta^{18}O$ of benthic foraminifera, which suggests an increase in deep ocean temperatures of about 5 °C from the mid-Paleocene to the peak warming of the EECO (Zachos et al., 2008). Our measured temperature increase of 7 °C from the Paleocene to the Eocene is larger than that observed in the deep ocean, although our uncertainty of ±3 °C (95% CI from a *t* test) permits this terrestrial estimate to be closer to the oceanic estimate. It is not

unreasonable for inland tropical temperatures to increase more than oceanic temperatures as a result of continentality (Rohling et al., 2012), an effect that has been noted in other terrestrial records from the Paleogene (e.g., Hyland et al., 2017; McInerney & Wing, 2011) and in the modern (Diffenbaugh & Field, 2013).

4.3. Increase in $\delta^{18}O_w$ From the Mid-Paleocene to the Late Paleocene/Early Eocene

We interpret the $\delta^{18}O_w$ data by taking the mean of the $\delta^{18}O$ values of several nodules from periods of time that appear to be similar or near constant. For $\delta^{18}O_w$, we divide the record at ~59 Ma (between nodules with ages of 59.7 and 58.4 Ma) because this breakpoint minimizes the misfit from the means (supporting information Text S1 and Figure S5). This analysis suggests that an apparent increase in $\delta^{18}O_w$ may have occurred ~2–3 Ma before the apparent increase in temperatures in the same record (which occurs at ~ 56 Ma). However, dividing the $\delta^{18}O_w$ record at 56 Ma only results in $<$1% increase in root mean square error (if the analysis is performed with sample replicate data; Figure S5). Therefore, these data are insufficient to justify speculation about lags between hydrologic and global temperature change.

We observe that the average $\delta^{18}O_w$ is 2.1 ± 0.9‰ higher in the late Paleocene/early Eocene than in the early to mid-Paleocene ($-$0.81 ± 0.35‰ and $-$ 2.8 ± 0.74‰, respectively, p = 0.00004 from a t test; Figure 4). We hypothesize that this increase in $\delta^{18}O_w$ relates to the contemporaneous increase in surface temperatures through one or more of the following processes: (1) increased evaporative enrichment in soil water, (2) increased $\delta^{18}O_w$ of the summertime rainfall, and/or (3) an increased proportion of summer rainfall recorded in the Eocene carbonates.

Increased evaporation of soil water can cause an increase in $\delta^{18}O_w$. Evaporative effects can increase soil water $\delta^{18}O_w$ values relative to local rainfall by up to ~10‰ in extreme conditions such as the Atacama desert (Quade, Rech, et al., 2007). As noted earlier, the Eocene soils in Big Bend are generally better drained than those from the Paleocene, so it is likely that soil waters in the Eocene were more enriched in ^{18}O due to enhanced evaporation. This evaporative effect could be partially offset by the observation that Eocene carbonates generally formed deeper in the soil than the Paleocene carbonates (Figure S1; also described in Bataille et al., 2016), although these apparent depths are imprecise due to indistinct soil tops and truncation. Increased evaporation likely contributes to the observed increase in $\delta^{18}O_w$ between the Paleocene and the Eocene.

It is also possible that the $\delta^{18}O$ of rainfall at Big Bend was higher during the Eocene than during the Paleocene and could contribute to increased $\delta^{18}O$ values of the soil water from which our carbonate samples precipitated. Higher local temperatures are spatially and temporally correlated with higher $\delta^{18}O$ values in the modern, although this relationship is relatively weak at low latitudes and in the summer when precipitation is more convective (Rozanski et al., 1993; Vachon et al., 2010). All else equal, an increase in condensation temperature of 10 °C would increase the $\delta^{18}O$ of rainfall by on the order of 3‰ (Vachon et al., 2010)—roughly the magnitude of the shift observed in both temperature and $\delta^{18}O_w$ across the Paleocene-Eocene boundary in our record. Additionally, an isotope-enabled general circulation model (GCM) predicts that the $\delta^{18}O$ value of the proto-Gulf of Mexico in the Eocene was about 1‰ higher than modern (after correcting for ice volumes; Tindall et al., 2010). Although the difference in $\delta^{18}O_w$ of the Gulf between the Paleocene and the Eocene was likely smaller than predicted for the difference between Eocene and modern, it is possible that a similar change in source water compositions could contribute to the enrichment in ^{18}O recorded by the soil carbonates.

Finally, the increase in reconstructed $\delta^{18}O_w$ from the Paleocene to the Eocene could also relate to an increase in the relative proportion of summertime rainfall recorded by those carbonates. Modern summer precipitation in western Texas comes primarily from the Gulf of Mexico through a monsoon-like system and is more enriched in ^{18}O than winter precipitation that originates primarily from frontal systems forced by cool air masses that have traveled overland from the Pacific (Licht et al., 2017; Nativ & Riggio, 1990; Vachon et al., 2010; Vera et al., 2006) (Figure S7). Recent work shows that soils yield carbonates with calculated $\delta^{18}O_w$ that resembles the $\delta^{18}O$ of rainfall during the months in which the carbonates grew (Gallagher & Sheldon, 2016; Hough et al., 2014). Thus, assuming that these moisture source patterns were similar to modern throughout the Paleogene (as Fricke et al., 2010, predict for the Cretaceous North America), an increase in $\delta^{18}O$ of rainfall in the Eocene could also be explained by preferential carbonate accumulation during summer rain events from moisture derived from the proto-Gulf of Mexico. Thus, it might be possible that a slight difference in

the timing of carbonate accumulation and/or timing of moisture traveling inland from the proto-Gulf could also contribute to the difference in $\delta^{18}O_w$ observed in the Eocene and Paleocene.

Although reconstructed soil water $\delta^{18}O_w$ values increase from the Paleocene to the Eocene, the average $\delta^{18}O_w$ values for those time periods are both similar to the $\delta^{18}O$ of modern summer rainfall in the region. The isotopic composition of modern rainfall in south Texas has a strong seasonal cycle (range of ~6‰; Figure S7; estimates from the Oxygen Isotopes in Precipitation Calculator, version 3.1, http://waterisotopes.org; Bowen & Revenaugh, 2003). We find a mean Paleogene $\delta^{18}O_w$ of -1.4‰, while modern rainfall in the region is about -3‰ in June and 0‰ in July and August. The similarity between mean Paleogene $\delta^{18}O_w$ reconstructed from the Big Bend carbonates and the $\delta^{18}O$ values of modern rainfall during summer months is consistent with the hypothesis that Paleocene and Eocene moisture patterns were not dissimilar from modern (Figure S7), given our interpretation of a summer bias of the clumped isotope proxy. The relatively high $\delta^{18}O$ of Paleogene Big Bend waters (-1.4‰) might suggest that the ancient North American summer monsoon did not impart a strong amount effect (a depletion in ^{18}O with intense rainfall) on the summer soil waters of this area. Similarly, the amount effect is not observed in modern summer precipitation in the North American monsoon (Eastoe & Dettman, 2016). These results suggest that the Paleocene/Eocene North American monsoon was not particularly more intense or more deeply convective than the modern monsoon, despite modeling predictions to the contrary (Held & Soden, 2006; Huber & Goldner, 2012; Keery et al., 2018; Licht et al., 2014).

Despite this result, it is possible that the predicted intense monsoons may have occurred during transient periods of extreme Paleocene-Eocene warmth that are not recorded in our pedogenic carbonate data. It has been hypothesized that hyperthermals during this period are represented in the stratigraphy as distinctive sand bodies in the Tornillo Basin (Bataille et al., 2016, 2018). Indeed, the spacing and thickness of the Tornillo Basin sandstones may be consistent with the hypothesis that intense seasonal precipitation during hyperthermals caused an increase in erosion and flushing of sediment, as described in other Laramide basins (Foreman, 2014; Foreman et al., 2012). If true, it is possible that the intense, convective hydrological cycle predicted for the early Eocene occurred during hyperthermals, but due to the absence of nodules in the sandstone units, our paleosol carbonate record in the Tornillo Basin is stratigraphically biased against these events.

4.4. Comparison to Previous Clumped Isotope Records in North America From the Paleogene and Modern Air Temperatures

Our clumped isotope data from the Tornillo Basin add to the existing sparse data available from terrestrial North America in the Paleogene, and examining these data together can elucidate variability and temperature differences with latitude. Here we compare our temperature results to temperature estimates produced from 14 late Paleocene and early Eocene carbonate nodules collected in the Bighorn Basin, WY (Snell et al., 2013) and 14 Early Eocene carbonate nodules collected in the Green River Basin, WY (Hyland et al., 2018; Figure 5).

Direct comparison of our results to the Δ_{47} values and temperature estimates from the Bighorn Basin reported by Snell et al. (2013) is complicated by recent developments in clumped isotope methods. The Δ_{47} data in Snell et al. (2013) were produced at Caltech between 2006 and 2011 when standard practice was to use the ^{17}O correction parameters of Santrock et al. (1985) for calculations and present data in the *Ghosh* or *Caltech* reference frame. Our Δ_{47} values are calculated using updated ^{17}O correction parameters (Brand et al., 2010) following recent recommendations (Daëron et al., 2016; Schauer et al., 2016) and are normalized to the absolute reference frame (Dennis et al., 2011), which is now standard practice. Unfortunately, the data do not exist to recalculate the earlier Snell et al. (2013) Δ_{47} values to make them quantitatively comparable to the Δ_{47} values presented here. Comparing the temperatures calculated from the Δ_{47} values in the two studies is actually more appropriate, because each study used the Δ_{47}-temperature calibration based on empirical data generated in the same laboratory and calculated using the same methods as their sample data. However, analytical differences make it inappropriate to use the same Δ_{47}-temperature calibration for both data sets, so this temperature comparison likely introduces unquantified error on the order of a couple of degrees.

The average clumped isotope temperature from the 14 Bighorn Basin carbonate nodules is 36 ± 3 °C (Snell et al., 2013). Snell et al. (2013) adjusted their clumped isotope soil temperature to account for radiative

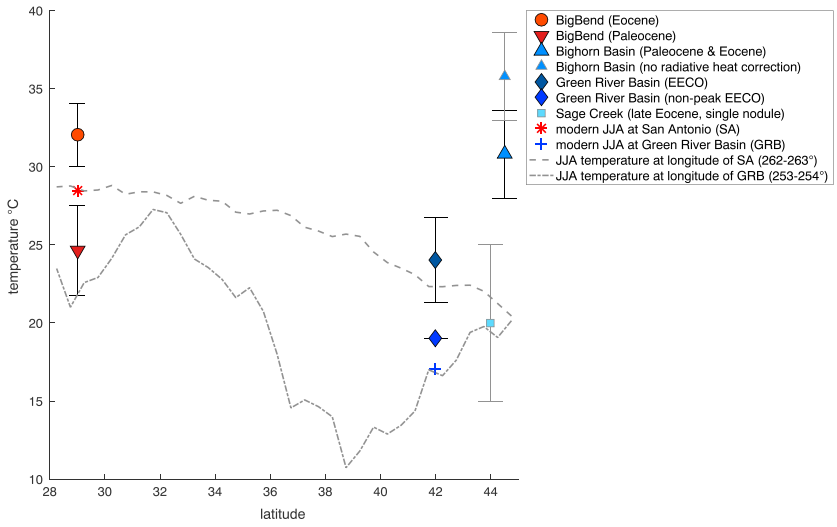

Figure 5. Clumped isotope temperatures (filled symbols) and modern June-July-August (JJA) average temperatures from NCEP/NCAR reanalysis data (Kalnay et al., 1996; star/cross symbols and dashed lines) versus latitude for relevant locations in North America. The error bars shown for the clumped isotope data are the 95% confidence interval of the mean of several nodules. The Green River Basin data are from the early Eocene climatic optimum (EECO; Hyland et al., 2018), and the Bighorn Basin data are from the late Paleocene and early Eocene (Snell et al., 2013), shown with and without the 5 °C correction for radiative heating. The late Eocene Sage Creek single nodule is from Methner et al. (2016).

heating of the soil surface: they subtracted 5 °C from the measured carbonate temperature, yielding an estimate of 31 ± 3 °C for summer air temperature. We do not adjust our temperature estimates for radiative heating because tree fossils indicate that the Tornillo Basin was forested (Lehman & Busbey, 2007; Wheeler, 1991; Wheeler & Lehman, 2005), and so it is unlikely that the soils experienced enough heating from incident solar radiation to cause large differences in soil versus air temperatures as has been observed for bare soils (Passey et al., 2010; Quade et al., 2013). The soils in the Bighorn Basin were likely not bare either (Wing et al., 2005, references within), but for comparison purposes, we adopt the authors' judgment with respect to the solar heating effect on their record (the average Bighorn Basin clumped isotope temperature without this adjustment is plotted for reference in Figure 5).

Direct comparison between the Tornillo and Green River Basin data is considerably simpler because the Green River Δ_{47} data were also produced at the University of Washington IsoLab, following the same procedures, and during the same time period, thus removing the concern of interlaboratory discrepancies or temperature calibration differences between these two data sets. The average clumped isotope values from the 14 carbonate nodules from the Green River Basin yield summer temperature estimates of 24 ± 3 °C including the peak warming of the EECO and 19 ± 1 °C excluding the peak-EECO samples (Hyland et al., 2018); these estimates are interpreted as summer temperatures by the authors (no correction for radiative heating). A single nodule from the latest Eocene in Sage Creek, MT provides a clumped isotope temperature estimate of 20 ± 5 °C (Methner et al., 2016) (Figure 5), which is similar to the temperature estimate from Green River; however, the Sage Creek estimate is more error-prone because it comes from a single nodule and thus is not discussed further.

Despite their similarity in latitude, the Bighorn Basin Δ_{47} data and the Green River Basin Δ_{47} data yield very different temperatures (Figure 5). It is possible that the disparity in temperatures between these basins is due to differences in paleo-elevation. Although many studies suggest that both basins were likely at $<$1 km in elevation during the Eocene (Fan et al., 2011; Fricke, 2003; Morrill & Koch, 2002), some data suggest surface uplift in the Cordillera in the earliest Eocene (Feng & Poulsen, 2016; Mix et al., 2011). The disparity between the Bighorn and Green River data could also be due to differences in radiative heating due to local topography or aspect, distance from bodies of water that could provide cooling, unaccounted for differences in the intra-annual timing of accumulation of the soil carbonates, or unquantifiable differences due to improvements in clumped isotope methods.

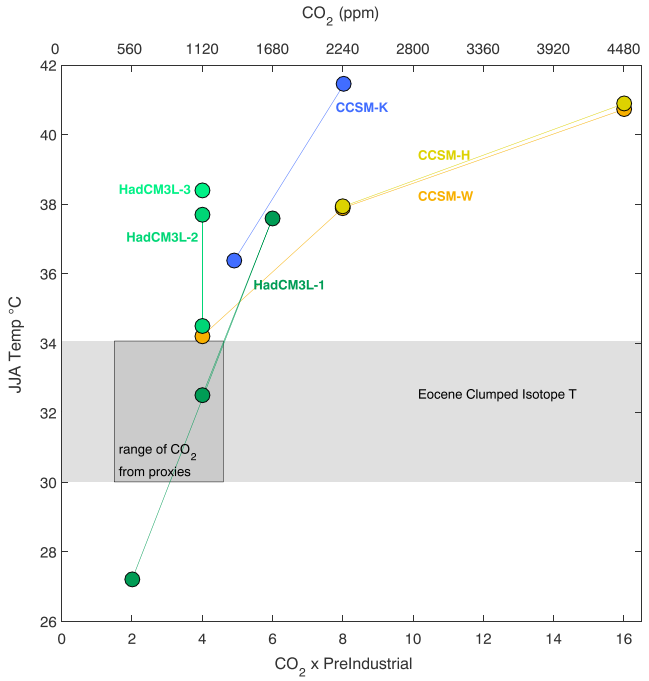

Figure 6. June-July-August (JJA) average temperature at Big Bend for Eocene general circulation model simulations with atmospheric CO_2 concentrations of 1 to 16× preindustrial CO_2. The horizontal dashed line is the Eocene clumped isotope temperature estimate from Big Bend, with the 95% confidence interval in light gray shading. The dark gray rectangle is the atmospheric CO_2 concentrations from Anagnostou et al. (2016). Model citations are as follows: CCSM-H, Huber and Caballero (2011); CCSM-K, Kiehl and Shields (2013); CCSM-W, Winguth et al. (2010); HadCM3L-1, Lunt et al. (2010); HadCM3L-2, Loptson et al. (2014); and HadCM3L-3, Lunt et al. (2016), Inglis et al. (2017), and Valdes et al. (2017).

The disparate temperatures from the midlatitude Bighorn and Green River Basins imply very different latitudinal gradients for Eocene North America when compared to our lower-latitude temperatures from the Tornillo Basin. The Eocene summer temperature estimate from the Tornillo Basin (32 ± 3 °C) is within error of the Bighorn Basin temperatures (31 ± 3 °C), which would imply a flat latitudinal temperature gradient (Figure 5). In contrast, the Tornillo Basin clumped isotope temperatures are hotter than the Green River Basin temperatures by 8 ± 4 °C (difference and 95% CI from a *t* test); this difference approximates the temperature difference that exists in the modern between sites at those two latitudes (i.e., mean June-July-August [JJA] temperatures in San Antonio and modern Green River Basin are 10 °C different; Figure 5), which would imply a latitudinal temperature gradient similar to modern.

The difficulty of reconstructing Paleogene latitudinal temperature gradients from local temperature reconstructions is not surprising given that land temperatures and latitudinal temperature gradients are heterogeneous, which can be illustrated by considering modern reanalysis data (Kalnay et al., 1996). While the modern latitudinal temperature gradient at the longitude of San Antonio (97°W) conforms to the simple prediction of decreasing temperatures with increasing latitude, the gradient at the longitude of the Green River Basin (107°W) does not, due to the influence of topography (Figure 5). Furthermore, modern JJA temperatures near Big Bend, TX (from the west coast of North America to the west coast of the Gulf of Mexico at latitudes of 29–30°N) range widely from 18–30 °C. Land cover likely contributes to significant variability in Earth surface temperatures (Thrasher & Sloan, 2010). These observations might explain why our estimated summer temperature for the forested Paleocene environment is slightly cooler than JJA temperature for modern San Antonio shrubland environment (Figure 5), even though the Paleogene was globally warmer than modern. San Antonio might also be cooler because it is not the correct locality to compare to the Tornillo Basin: we use it here due to similar latitude and distance to the coast, but the variability in local temperatures suggests that there are other factors that control surface temperature. Given inherent variability in surface temperatures on land, a more complete understanding of summer temperatures in the Eocene in North America could emerge with refinement of paleotopography, paleovegetation, and additional clumped isotope data from basins over a larger range in longitudes and latitudes.

4.5. Comparison to Predictions From Eocene General Circulation Models

The temperature record from the Tornillo Basin provides an opportunity to test model predictions for temperatures on land at subtropical latitudes. While it is common to average several model grid cells centered on the preferred proxy location (e.g., Snell et al., 2013), at Tornillo Basin, that method would involve including cells that are different in temperature due to differing distance from the coast. The range in temperatures predicted in grid cells surrounding Big Bend is larger than the range in temperatures predicted at a single cell by various simulations of a general circulation model from the UK Met Office (HadCM3L, Figure S8). With this caveat in mind, we compare our $T\Delta_{47}$ estimate from the Tornillo Basin to predictions from available Eocene GCMs (most of which are described in Lunt et al., 2012) using JJA temperature from the grid cell that best approximates the paleolocation of the Tornillo Basin (Figure S8).

Most of the Eocene GCMs presented here predict summer temperatures that are hotter than our estimate from clumped isotopes (Figure 6). Only three of 13 simulations predict temperatures that are within error of our clumped isotope temperatures: HadCM3L-1 (Lunt et al., 2010) for the ×4 CO_2 forcing scenario, HadCM3L-2 (Loptson et al., 2014) for the ×4 CO_2 forcing scenario with homogeneous shrubs, and CCSM-W (Winguth et al., 2010) for the ×4 CO_2 forcing scenario (Figure 6). The HadCM3L simulations that predict temperatures higher than our maximum proxy estimate are run at higher pCO_2 forcings (×6 CO_2;

HadCM3L-1, Lunt et al., 2010), with dynamic vegetation (HadcM3L-2, Loptson et al., 2014) or with varied paleogeography (HadCM3L-3; Inglis et al., 2017; Valdes et al., 2017). The CCSM-H and CCSM-W simulations (Huber & Caballero, 2011; Winguth et al., 2010) overestimate our proxy-derived summer temperatures at Tornillo Basin by 2–4 °C. The CCSM-K simulations (Kiehl & Shields, 2013) overestimate the Tornillo Basin temperatures by 2–6 °C with lower CO_2 forcing; those simulations have modified aerosol parameters that change cloud condensation properties to reduce discrepancies with high-latitude proxy data.

In summary, some simulations predict summer temperatures that are within error of our estimates (Figure 6), but most simulations predict summer temperatures that are higher than the low-latitude terrestrial temperatures estimated here. These temperature discrepancies of 2–7 °C are similar in size to those reported between low-latitude sea surface temperature proxies and models (Evans et al., 2018). The simulations that predict warmer temperatures than our low-latitude terrestrial proxy estimates and the low-latitude sea surface temperature estimates from Evans et al. (2018) are the same simulations that have been interpreted as generally agreeing with proxy data from high latitudes or with proxy-based marine latitudinal temperature gradients (see Huber & Caballero, 2011; Kiehl & Shields, 2013; Loptson et al., 2014). Thus, our data provide additional evidence that in order to match the proxy latitudinal temperature gradients and/or high-latitude temperatures predicted by proxies, models tend to overheat lower latitude temperatures (Evans et al., 2018; Keating-Bitonti et al., 2011; Kozdon et al., 2011; Pearson et al., 2001; Spicer et al., 2014; Tripati et al., 2003). Our results imply that the summer surface temperatures of $>$36 °C predicted by models are unlikely for this coastal environment and that temperatures lower than the thermal threshold for survival of organisms occurred at least locally during greenhouse climates. Our results suggest that coastal, subtropical climates remained relatively mild throughout background greenhouse climates and thus proxy-model discrepancy persists at low latitudes.

5. Conclusions

We measure the $\delta^{13}C$, $\delta^{18}O$, and Δ_{47} composition of paleosol carbonate nodules from the Paleocene to the early Eocene from the Tornillo Basin in Big Bend National Park, Texas (USA). These analyses provide insight into a subtropical, near-coastal environment during a greenhouse climate regime. We find that most of our measured carbonate nodules record primary environmental signals and two of our nodules have been reset by thermal heating from an adjacent laccolith. We estimate an average $T\Delta_{47}$ of 25 ± 3 °C through the Paleocene and a statistically significant increase to 32 ± 2 °C in the early Eocene. The increase in temperature recorded across this interval also corresponds to an increase in the calculated $\delta^{18}O$ of soil water from −2.8 ± 0.74 to −0.81 ± 0.35‰ (standard mean ocean water) that occurs at ~59 Ma. The shift in temperatures and water compositions is likely correlated with increasing atmospheric CO_2 (Anagnostou et al., 2016; Beerling & Royer, 2011).

Our data provide quantitative constraints on subtropical temperatures during the Paleocene and early Eocene that can inform our understanding of greenhouse climates. A comparison between the summer temperature estimate from the Tornillo Basin Δ_{47} data and similar data from the Bighorn Basin and the Green River Basin demonstrates the complexity and heterogeneity of terrestrial temperature records. Reliable estimates of latitudinal temperature gradients on land likely await more data. While some Eocene GCM simulations agree within error of our estimate of summer temperature in the Tornillo Basin, most simulations overestimate summer temperature at this locality. The simulations that overestimate summer temperature are the simulations that have previously been interpreted as improvements to modeling Eocene climate because they show general agreement with other proxy estimates of latitudinal temperature gradients or temperatures from high latitudes. The tendency of these models to overestimate terrestrial subtropical paleotemperatures from Tornillo Basin mimics their tendency to overestimate low-latitude sea surface temperatures. Our results suggest that discrepancies remain between Eocene climate models and proxy data at low latitudes.

Acknowledgments
J. R. K. was supported by the National Science Foundation Graduate Research Fellowship Program under grant DGE-125082. Laboratory analyses were supported by the US NSF grants EAR-1156134 and EAR-1252064 to K. W. H. C. P. B. was supported by the University of Ottawa Faculty of Science startup funds. Work by the University of Utah group was supported by ACS-PRF award 52222-ND2 and US NSF grant EAR-1502786 to G. J. B. We gratefully acknowledge funding from the Quaternary Research Center and the Earth and Space Sciences Department at the University of Washington. Thanks to Andrew Schauer for endless support in IsoLab and to Landon Burgener for field assistance. Samples in Big Bend National Park were collected under NPS permits BIBE-2016-SCI-0024 and BIBE-2014-SCI-0015; thanks to Don Corrick for assistance in the permitting process. Thanks to Dan Peppe, an anonymous reviewer, and Associate Editor Stephen Barker for suggestions that improved this manuscript. Isotope data including individual replicate analyses, carbonate standards, and reference frame gases can be found in the supporting information tables.

References

Affek, H. P. (2012). Clumped isotope paleothermometry: Principles, applications, and challenges. *The Paleontological Society Papers*, *18*, 101–114.

Anagnostou, E., John, E. H., Edgar, K. M., Foster, G. L., Ridgwell, A., Inglis, G. N., et al. (2016). Changing atmospheric CO_2 concentration was the primary driver of early Cenozoic climate. *Nature*, *533*(7603), 1–19. https://doi.org/10.1038/nature17423

Anhäuser, T., Hook, B. A., Halfar, J., Greule, M., & Keppler, F. (2018). Earliest Eocene cold period and polar amplification—Insights from δ^2H values of lignin methoxyl groups of mummified wood. *Palaeogeography, Palaeoclimatology, Palaeoecology*, *505*, 326–336. https://doi.org/10.1016/J.PALAEO.2018.05.049

Atchley, S. C., Nordt, L. C., & Dworkin, S. I. (2004). Eustatic control on alluvial sequence stratigraphy: A possible example from the Cretaceous-Tertiary transition of the Tornillo Basin, Big Bend National Park, West Texas, U.S.A. *Journal of Sedimentary Research*, *74*(3), 391–404. https://doi.org/10.1306/102203740391

Aze, T., Pearson, P. N., Dickson, A. J., Badger, M. P. S., Bown, P. R., Pancost, R. D., et al. (2014). Extreme warming of tropical waters during the Paleocene-Eocene Thermal Maximum. *Geology*, *42*(9), 739–742. https://doi.org/10.1130/G35637.1

Bataille, C. P., Ridgeway, K. D., Colliver, L., & Liu, X.-M. (2018). *An early Paleogene fluvial regime shift in response to global warming: A subtropical record from the Tornillo basin, West Texas*. U.S.A: The Geological Society of America Bulletin. https://doi.org/10.1130/B31872.1

Bataille, C. P., Watford, D., Ruegg, S., Lowe, A., & Bowen, G. J. (2016). Chemostratigraphic age model for the Tornillo Group: A possible link between fluvial stratigraphy and climate. *Palaeogeography, Palaeoclimatology, Palaeoecology*, *457*, 277–289. https://doi.org/10.1016/j.palaeo.2016.06.023

Beerling, D. J., & Royer, D. L. (2011). Convergent Cenozoic CO_2 history. *Nature Geoscience*, *4*(7), 418–420. https://doi.org/10.1038/ngeo1186

Bernard, S., Daval, D., Ackerer, P., Pont, S., & Meibom, A. (2017). Burial-induced oxygen-isotope re-equilibration of fossil foraminifera explains ocean paleotemperature paradoxes. *Nature Communications*, *8*(1), 1–10. https://doi.org/10.1038/s41467-017-01225-9

Bernasconi, S. M., Müller, I. A., Bergmann, K. D., Breitenbach, S. F. M., Fernandez, A., Hodell, D. A., et al. (2018). Reducing uncertainties in carbonate clumped isotope analysis through consistent carbonate-based standardization. *Geochemistry, Geophysics, Geosystems*, *19*. https://doi.org/10.1029/2017GC007385

Bijl, P. K., Schouten, S., Sluijs, A., Reichart, G. J., Zachos, J. C., & Brinkhuis, H. (2009). Early Palaeogene temperature evolution of the southwest Pacific Ocean. *Nature*, *461*(7265), 776–779. https://doi.org/10.1038/nature08399

Bonifacie, M., Calmels, D., Eiler, J. M., Horita, J., Chaduteau, C., Vasconcelos, C., et al. (2017). Calibration of the dolomite clumped isotope thermometer from 25 to 350 °C, and implications for a universal calibration for all (Ca, Mg, Fe)CO_3 carbonates. *Geochimica et Cosmochimica Acta*, *200*, 255–279. https://doi.org/10.1016/J.GCA.2016.11.028

Bowen, G., & Revenaugh, J. (2003). Interpolating the isotopic composition of modern meteoric precipitation. *Water Resources Research*, *39*(10), 1299. https://doi.org/10.1029/2003WR002086

Brand, W. A., Assonov, S. S., & Coplen, T. B. (2010). Correction for the ^{17}O interference in $\delta(^{13}C)$ measurements when analyzing CO_2 with stable isotope mass spectrometry (IUPAC technical report). *Pure and Applied Chemistry*, *82*(8), 1719–1733. https://doi.org/10.1351/PAC-REP-09-01-05

Breecker, D. O., Sharp, Z. D., & McFadden, L. D. (2009). Seasonal bias in the formation and stable isotopic composition of pedogenic carbonate in modern soils from central New Mexico, USA. *Bulletin of the Geological Society of America*, *121*(3), 630–640. https://doi.org/10.1130/B26413.1

Brinkhuis, H., Schouten, S., Collinson, M. E., Sluijs, A., Damsté, J. S. S., Dickens, G. R., et al. (2006). Episodic fresh surface waters in the Eocene Arctic Ocean. *Nature*, *441*(7093), 606–609. https://doi.org/10.1038/nature04692

Burgener, L., Huntington, K. W., Hoke, G. D., Schauer, A., Ringham, M. C., Latorre, C., et al. (2016). Variations in soil carbonate formation and seasonal bias over >4 km of relief in the western Andes (30°S) revealed by clumped isotope thermometry. *Earth and Planetary Science Letters*, *441*, 188–199. https://doi.org/10.1016/j.epsl.2016.02.033

Carmichael, M. J., Inglis, G. N., Badger, M. P. S., Naafs, B. D. A., Behrooz, L., Remmelzwaal, S., et al. (2017). Hydrological and associated biogeochemical consequences of rapid global warming during the Paleocene-Eocene Thermal Maximum. *Global and Planetary Change*, *157*, 114–138. https://doi.org/10.1016/j.gloplacha.2017.07.014

Carmichael, M. J., Lunt, D., & Pancost, R. (2015). Insights into the early Eocene hydrological cycle from an ensemble of atmosphere-ocean GCM simulations, EGU General Assembly 2015. *17*, 8839. https://doi.org/10.5194/cpd-11-3277-2015

Carmichael, M. J., Lunt, D. J., Huber, M., Heinemann, M., Kiehl, J., LeGrande, A., et al. (2016). A model-model and data-model comparison for the early Eocene hydrological cycle. *Climate of the Past*, *12*(2), 455–481. https://doi.org/10.5194/cp-12-455-2016

Cui, Y., & Schubert, B. A. (2017). Atmospheric pCO_2 reconstructed across five early Eocene global warming events. *Earth and Planetary Science Letters*, *478*, 225–233. https://doi.org/10.1016/J.EPSL.2017.08.038

Daëron, M., Blamart, D., Peral, M., & Affek, H. P. (2016). Absolute isotopic abundance ratios and the accuracy of Δ_{47} measurements. *Chemical Geology*, *442*, 83–96. https://doi.org/10.1016/j.chemgeo.2016.08.014

Dennis, K. J., Affek, H. P., Passey, B. H., Schrag, D. P., & Eiler, J. M. (2011). Defining an absolute reference frame for 'clumped' isotope studies of CO_2. *Geochimica et Cosmochimica Acta*, *75*(22), 7117–7131. https://doi.org/10.1016/j.gca.2011.09.025

Diffenbaugh, N. S., & Field, C. B. (2013). Changes in ecologically critical terrestrial climate conditions. *Science*, *341*(6145), 486–492. https://doi.org/10.1126/science.1237123

Eastoe, C. J., & Dettman, D. L. (2016). Isotope amount effects in hydrologic and climate reconstructions of monsoon climates: Implications of some long-term data sets for precipitation. *Chemical Geology*, *430*, 78–89. https://doi.org/10.1016/j.chemgeo.2016.03.022

Eberle, J. J., Fricke, H. C., Humphrey, J. D., Hackett, L., Newbrey, M. G., & Hutchison, J. H. (2010). Seasonal variability in Arctic temperatures during early Eocene time. *Earth and Planetary Science Letters*, *296*(3–4), 481–486. https://doi.org/10.1016/j.epsl.2010.06.005

Eberle, J. J., & Greenwood, D. R. (2012). Life at the top of the greenhouse Eocene world—A review of the Eocene flora and vertebrate fauna from Canada's high Arctic. *GSA Bulletin*, *124*(1–2), 3–23. https://doi.org/10.1130/B30571.1

Eiler, J. M. (2007). "Clumped-isotope" geochemistry—The study of naturally-occurring, multiply-substituted isotopologues. *Earth and Planetary Science Letters*, *262*(3–4), 309–327. https://doi.org/10.1016/j.epsl.2007.08.020

Eiler, J. M. (2011). Paleoclimate reconstruction using carbonate clumped isotope thermometry. *Quaternary Science Reviews*, *30*(25–26), 3575–3588. https://doi.org/10.1016/j.quascirev.2011.09.001

Evans, D., Sagoo, N., Renema, W., Cotton, L. J., Müller, W., Todd, J. A., et al. (2018). Eocene greenhouse climate revealed by coupled clumped isotope-Mg/Ca thermometry. *Proceedings of the National Academy of Sciences*, *115*(6), 1174–1179. https://doi.org/10.1073/pnas.1714744115

Fan, M., DeCelles, P. G., Gehrels, G. E., Dettman, D. L., Quade, J., & Peyton, S. L. (2011). Sedimentology, detrital zircon geochronology, and stable isotope geochemistry of the lower Eocene strata in the Wind River Basin, central Wyoming. *GSA Bulletin*, *123*(5–6), 979–996. https://doi.org/10.1130/B30235.1

Feng, R., & Poulsen, C. J. (2016). Refinement of Eocene lapse rates, fossil-leaf altimetry, and North American cordilleran surface elevation estimates. *Earth and Planetary Science Letters*, *436*, 130–141. https://doi.org/10.1016/j.epsl.2015.12.022

Fernandez, A., Müller, I. A., Rodríguez-Sanz, L., van Dijk, J., Looser, N., & Bernasconi, S. M. (2017). A reassessment of the precision of carbonate clumped isotope measurements: Implications for calibrations and paleoclimate reconstructions. *Geochemistry, Geophysics, Geosystems*, *18*, 375–4386. https://doi.org/10.1002/2017GC007106

Finnegan, S., Bergmann, K., Eiler, J. M., Jones, D. S., Fike, D. A., Eisenman, I., et al. (2011). The magnitude and duration of Late Ordovician-Early Silurian glaciation. *Science*, *331*(6019), 903–906. https://doi.org/10.1126/science.1200803

Foreman, B. Z. (2014). Climate-driven generation of a fluvial sheet sand body at the Paleocene-Eocene boundary in north-west Wyoming (USA). *Basin Research*, *26*(2), 225–241. https://doi.org/10.1111/bre.12027

Foreman, B. Z., Heller, P. L., & Clementz, M. T. (2012). Fluvial response to abrupt global warming at the Palaeocene/Eocene boundary. *Nature*, *491*(7422), 92–95. https://doi.org/10.1038/nature11513

Fricke, H. C. (2003). Investigation of early Eocene water-vapor transport and paleoelevation using oxygen isotope data from geographically widespread mammal remains. *Geological Society of America Bulletin*, *9*, 1088–1096.

Fricke, H. C., Foreman, B. Z., & Sewall, J. O. (2010). Integrated climate model-oxygen isotope evidence for a North American monsoon during the Late Cretaceous. *Earth and Planetary Science Letters*, *289*(1–2), 11–21. https://doi.org/10.1016/J.EPSL.2009.10.018

Frieling, J., Gebhardt, H., Huber, M., Adekeye, O. A., Akande, S. O., Reichart, G. J., et al. (2017). Extreme warmth and heat-stressed plankton in the tropics during the Paleocene-Eocene Thermal Maximum. *Science Advances*, *3*(3). https://doi.org/10.1126/sciadv.1600891

Gallagher, T. M., & Sheldon, N. D. (2016). Combining soil water balance and clumped isotopes to understand the nature and timing of pedogenic carbonate formation. *Chemical Geology*, *435*, 79–91. https://doi.org/10.1016/j.chemgeo.2016.04.023

Galloway, W. E., Whiteaker, T. L., & Ganey-curry, P. (2011). History of Cenozoic North American drainage basin evolution, sediment yield, and accumulation in the Gulf of Mexico basin. *Geosphere*, *7*(4), 938–973. https://doi.org/10.1130/GES00647.1

Ghosh, P., Adkins, J., Affek, H., Balta, B., Guo, W., Schauble, E. A., et al. (2006). ^{13}C–^{18}O bonds in carbonate minerals: A new kind of paleothermometer. *Geochimica et Cosmochimica Acta*, *70*(6), 1439–1456. https://doi.org/10.1016/j.gca.2005.11.014

Greenwood, D. R., & Wing, S. L. (1995). Eocene continental climates and latitudinal temperature gradients. *Geology*, *23*(11), 1044–1048. https://doi.org/10.1130/0091-7613(1995)023<1044:ECCALT>2.3.CO;2

Harrington, G. J., & Jaramillo, C. A. (2007). Paratropical floral extinction in the Late Palaeocene-Early Eocene. *Journal of the Geological Society*, *164*(2), 323–332. https://doi.org/10.1144/0016-76492006-027

Haywood, A. M., Ridgwell, A., Lunt, D. J., Hill, D. J., Pound, M. J., Dowsett, H. J., et al. (2011). Are there pre-Quaternary geological analogues for a future greenhouse warming? *Philosophical Transactions of the Royal Society A: Mathematical, Physical and Engineering Sciences*, *369*(1938), 933–956. https://doi.org/10.1098/rsta.2010.0317

Head, J. J., Bloch, J. I., Hastings, A. K., Bourque, J. R., Cadena, E. A., Herrera, F. A., et al. (2009). Giant boid snake from the Palaeocene neotropics reveals hotter past equatorial temperatures. *Nature*, *457*(7230), 715–717. https://doi.org/10.1038/nature07671

Heinemann, M., Jungclaus, J. H., & Marotzke, J. (2009). Warm Paleocene/Eocene climate as simulated in ECHAM5/MPI-OM. *Climate of the Past*, *5*(4), 785–802. https://doi.org/10.5194/cp-5-785-2009

Held, I. M., & Soden, B. J. (2006). Robust responses of the hydrological cycle to global warming. *Journal of Climate*, *19*(21), 5686–5699. https://doi.org/10.1175/JCLI3990.1

Henkes, G. A., Passey, B. H., Grossman, E. L., Shenton, B. J., Pérez-Huerta, A., & Yancey, T. E. (2014). Temperature limits for preservation of primary calcite clumped isotope paleotemperatures. *Geochimica et Cosmochimica Acta*, *139*, 362–382. https://doi.org/10.1016/j.gca.2014.04.040

Ho, S. L., & Laepple, T. (2016). Flat meridional temperature gradient in the early Eocene in the subsurface rather than surface ocean. *Nature Geoscience*, *9*(8), 606–610. https://doi.org/10.1038/ngeo2763

Hollis, C. J., Handley, L., Crouch, E. M., Morgans, H. E. G., Baker, J. A., Creech, J., et al. (2009). Tropical sea temperatures in the high-latitude South Pacific during the Eocene. *Geology*, *37*(2), 99–102. https://doi.org/10.1130/G25200A.1

Hollis, C. J., Taylor, K. W. R., Handley, L., Pancost, R. D., Huber, M., Creech, J. B., et al. (2012). Early Paleogene temperature history of the Southwest Pacific Ocean: Reconciling proxies and models. *Earth and Planetary Science Letters*, *349–350*, 53–66. https://doi.org/10.1016/j.epsl.2012.06.024

Hough, B. G., Fan, M., & Passey, B. H. (2014). Calibration of the clumped isotope geothermometer in soil carbonate in Wyoming and Nebraska, USA: Implications for paleoelevation and paleoclimate reconstruction. *Earth and Planetary Science Letters*, *391*. https://doi.org/10.1016/j.epsl.2014.01.008

Huber, M. (2008). A hotter greenhouse? *Science*, *321*, 353–354. https://doi.org/10.1126/science.1161170

Huber, M., & Caballero, R. (2011). The early Eocene equable climate problem revisited. *Climate of the Past*, *7*(2), 603–633. https://doi.org/10.5194/cp-7-603-2011

Huber, M., & Goldner, A. (2012). Eocene monsoons. *Journal of Asian Earth Sciences*, *44*, 3–23. https://doi.org/10.1016/J.JSEAES.2011.09.014

Huntington, K. W., Eiler, J. M., Affek, H. P., Guo, W., Bonifacie, M., Yeung, L. Y., et al. (2009). Methods and limitations of "clumped" CO_2 isotope ($\Delta 47$) analysis by gas-source isotope ratio mass spectrometry. *Journal of Mass Spectrometry*, *44*(9), 1318–1329. https://doi.org/10.1002/jms.1614

Huntington, K. W., & Lechler, A. R. (2015). Carbonate clumped isotope thermometry in continental tectonics. *Tectonophysics*, *647–648*, 1–20. https://doi.org/10.1016/j.tecto.2015.02.019

Hyland, E. G., Huntington, K. W., Sheldon, N. D., & Reichgelt, T. (2018). Temperature seasonality in the North American continental interior during the early Eocene climatic optimum. *Climate of the Past Discussions*, 1–39. https://doi.org/10.5194/cp-2018-28

Hyland, E. G., & Sheldon, N. D. (2013). Coupled CO_2-climate response during the early Eocene climatic optimum. *Palaeogeography, Palaeoclimatology, Palaeoecology*, *369*, 125–135. https://doi.org/10.1016/j.palaeo.2012.10.011

Hyland, E. G., Sheldon, N. D., & Cotton, J. M. (2017). Constraining the early Eocene climatic optimum: A terrestrial interhemispheric comparison. *Geological Society of America Bulletin*, *129*, 244–252. https://doi.org/10.1130/B31493.1

Inglis, G. N., Collinson, M. E., Riegel, W., Wilde, V., Farnsworth, A., Lunt, D. J., et al. (2017). Mid-latitude continental temperatures through the early Eocene in western Europe. *Earth and Planetary Science Letters*, *460*, 86–96. https://doi.org/10.1016/j.epsl.2016.12.009

Jagniecki, E. A., Lowenstein, T. K. T. K., Jenkins, D. M., & Demicco, R. V. (2015). Eocene atmospheric CO_2 from the nahcolite proxy. *Geology*, *43*(12), 1075–1078. https://doi.org/10.1130/G36886.1

Jaramillo, C. A., Rueda, M. J., & Mora, G. (2006). Cenozoic plant diversity in the Neotropics. *Science*, *311*, 1893–1896. https://doi.org/10.1126/science.1121380

Kalnay, E., Kanamitsu, M., Kistler, R., Collins, W., Deaven, D., Gandin, L., et al. (1996). The NCEP/NCAR 40-year reanalysis project. *Bulletin of the American Meteorological Society*, *77*(3), 437–472. https://doi.org/10.1175/1520-0477(1996)077<0437:TNYRP>2.0.CO;2

Keating-Bitonti, C. R., Ivany, L. C., Affek, H. P., Douglas, P., & Samson, S. D. (2011). Warm, not super-hot, temperatures in the early Eocene subtropics. *Geology*, *39*(8), 771–774. https://doi.org/10.1130/G32054.1

Keery, J. S., Holden, P. B., & Edwards, N. R. (2018). Sensitivity of the Eocene climate to CO_2 and orbital variability. *Climate of the Past Discussions*, *14*, 215–238. https://doi.org/10.5194/cp-2017-60

Kelson, J. R., Huntington, K. W., Schauer, A. J., Saenger, C., & Lechler, A. R. (2017). Toward a universal carbonate clumped isotope calibration: Diverse synthesis and preparatory methods suggest a single temperature relationship. *Geochimica et Cosmochimica Acta*, *197*. https://doi.org/10.1016/j.gca.2016.10.010

Kiehl, J. T., & Shields, C. A. (2013). Sensitivity of the Palaeocene-Eocene Thermal Maximum climate to cloud properties. *Philosophical Transactions of the Royal Society A: Mathematical, Physical and Engineering Sciences*, *371*(2001). 20130093. https://doi.org/10.1098/rsta.2013.0093

Kim, S. T., & O'Neil, J. R. (1997). Equilibrium and nonequilibrium oxygen isotope effects in synthetic carbonates. *Geochimica et Cosmochimica Acta*, *61*(16), 3461–3475. https://doi.org/10.1016/S0016-7037(97)00169-5

Kozdon, R., Kelly, D. C., Kita, N. T., Fournelle, J. H., & Valley, J. W. (2011). Planktonic foraminiferal oxygen isotope analysis by ion microprobe technique suggests warm tropical sea surface temperatures during the early Paleogene. *Paleoceanography*, *26*, PA3206. https://doi.org/10.1029/2010PA002056

Kraus, M. J., & Riggins, S. (2007). Transient drying during the Paleocene–Eocene Thermal Maximum (PETM): Analysis of paleosols in the bighorn basin, Wyoming. *Palaeogeography, Palaeoclimatology, Palaeoecology*, *245*(3–4), 444–461. https://doi.org/10.1016/j.palaeo.2006.09.011

Kraus, M. J., Woody, D. T., Smith, J. J., & Dukic, V. (2015). Alluvial response to the Paleocene–Eocene thermal maximum climatic event, polecat bench, Wyoming (U.S.A.). *Palaeogeography, Palaeoclimatology, Palaeoecology*, *435*, 177–192. https://doi.org/10.1016/J.PALAEO.2015.06.021

Krueger, R. C. (2017). Fluvial response to warming during the early Eocene Climatic Optimum, Green River Basin, Wyoming. Northern Arizona University, ProQuest Dissertations Publishing, 2018.10742725.

Lauretano, V., Littler, K., Polling, M., Zachos, J. C., & Lourens, L. J. (2015). Frequency, magnitude and character of hyperthermal events at the onset of the early Eocene climatic optimum. *Climate of the Past*, *11*(10), 1313–1324. https://doi.org/10.5194/cp-11-1313-2015

Lehman, T. M. (1990). Paleosols and the Cretaceous/Tertiary transition in the Big Bend region of Texas. *Geology*, *18*(4), 362–364. https://doi.org/10.1130/0091-7613(1990)018<0362:PATCTT>2.3.CO;2

Lehman, T. M. (1991). Sedimentation in the Laramide Tornillo Basin of West Texas. *Geological Society of America, Rocky Mountain Section; Abstracts with Programs*., *23*(4), 41.

Lehman, T. M., & Busbey, A. B. (2007). Big Bend field trip guide. Society of Vertebtrate Paleontology, 67th Annual Meeting, Field Trip Guidebook.

Lehman, T. M., Wick, S. L., Beatty, H. L., Straight, W. H., & Wagner, J. R. (2018). Stratigraphy and depositional history of the Tornillo Group (Upper Cretaceous-Eocene) of West Texas. *Geosphere*, *14*(5), 2206–2244. https://doi.org/10/1130/GESO1641.1

Leslie, C. E., Peppe, D. J., Williamson, T. E., Heizler, M., Jackson, M., Atchley, S. C., et al. (2018). Revised age constraints for Late Cretaceous to early Paleocene terrestrial strata from the Dawson Creek section, Big Bend National Park, west Texas. *Geological Society of America Bulletin*, 1–21. https://doi.org/10.1130/B31785.1

Licht, A., Quade, J., Kowler, A., De Los Santos, M., Hudson, A., Schauer, A., et al. (2017). Impact of the North American monsoon on isotope paleoaltimeters: Implications for the paleoaltimetry of the American Southwest. *American Journal of Science*, *317*, 1–33. https://doi.org/10.2475/01.2017.01

Licht, A., Van Cappelle, M., Abels, H. A., Ladant, J. B., Trabucho-Alexandre, J., France-Lanord, C., et al. (2014). Asian monsoons in a late Eocene greenhouse world. *Nature*, *513*(7519), 501–506. https://doi.org/10.1038/nature13704

Lloyd, M. K., Eiler, J. M., & Nabelek, P. I. (2017). Clumped isotope thermometry of calcite and dolomite in a contact metamorphic environment. *Geochimica et Cosmochimica Acta*, *197*, 323–344. https://doi.org/10.1016/j.gca.2016.10.037

Loptson, C. A., Lunt, D. J., & Francis, J. E. (2014). Investigating vegetation-climate feedbacks during the early Eocene. *Climate of the Past*, *10*(2), 419–436. https://doi.org/10.5194/cp-10-419-2014

Lowenstein, T. K., & Demicco, R. V. (2006). Elevated Eocene atmospheric CO_2 and its subsequent decline. *Science*, *313*(5795), 1928. https://doi.org/10.1126/science.1129555

Lunt, D. J., Elderfield, H., Pancost, R., Ridgwell, A., Foster, G. L., Haywood, A., et al. (2013). Warm climates of the past—A lesson for the future? *Philosophical Transactions of the Royal Society A: Mathematical, Physical and Engineering Sciences*, *371*(2001), 20130146. https://doi.org/10.1098/rsta.2013.0146

Lunt, D. J., Farnsworth, A., Loptson, C., Foster, G. L., Markwick, P., O'Brien, C. L., et al. (2016). Palaeogeographic controls on climate and proxy interpretation. *Climate of the Past*, *12*(5), 1181–1198. https://doi.org/10.5194/cp-12-1181-2016

Lunt, D. J., Jones, T. D., Heinemann, M., Huber, M., LeGrande, A., Winguth, A., et al. (2012). A model-data comparison for a multi-model ensemble of early Eocene atmosphere-ocean simulations: EoMIP. *Climate of the Past*, *8*(5), 1717–1736. https://doi.org/10.5194/cp-8-1717-2012

Lunt, D. J., Valdes, P. J., Jones, T. D., Ridgwell, A., Haywood, A. M., Schmidt, D. N., et al. (2010). CO_2-driven ocean circulation changes as an amplifier of Paleocene-Eocene thermal maximum hydrate destabilization. *Geology*, *38*(10), 875–878. https://doi.org/10.1130/G31184.1

Matthew, H., & Sloan, L. C. (2001). Heat transport, deep waters, and thermal gradients: Coupled simulation of an Eocene greenhouse climate. *Geophysical Research Letters*, *28*(18), 3481–3484. https://doi.org/10.1029/2001GL012943

Maxbauer, D. P., Royer, D. L., & LePage, B. A. (2014). High Arctic forests during the middle Eocene supported by moderate levels of atmospheric CO_2. *Geology*, *42*(12), 1027–1030. https://doi.org/10.1130/G36014.1

McInerney, F.a., & Wing, S. L. (2011). The Paleocene-Eocene thermal maximum: A perturbation of carbon cycle, climate, and biosphere with implications for the future. *Annual Review of Earth and Planetary Sciences*, *39*(1), 489–516. https://doi.org/10.1146/annurev-earth-040610-133431

Meckler, A. N., Ziegler, M., Millán, M. I., Breitenbach, S. F. M., & Bernasconi, S. M. (2014). Long-term performance of the Kiel carbonate device with a new correction scheme for clumped isotope measurements. *Rapid Communications in Mass Spectrometry*, *28*(15), 1705–1715. https://doi.org/10.1002/rcm.6949

Methner, K., Mulch, A., Fiebig, J., Wacker, U., Gerdes, A., Graham, S. A., et al. (2016). Rapid middle Eocene temperature change in western North America. *Earth and Planetary Science Letters*, *450*, 132–139. https://doi.org/10.1016/j.epsl.2016.05.053

Miggins, D., Anthony, E., Ren, M., & Wache, K. (2007). New $^{40}Ar/^{39}Ar$ ages, geochemistry, and stratigraphy for mafic and rhyolitic volcanic units from Big Bend National Park. In *Geological Society of America Abstracts with Programs* (Vol. 39, p. 635).

Mintz, J. S., Driese, S. G., Breecker, D. O., & Ludvigson, G. A. (2011). Influence of changing hydrology on pedogenic calcite precipitation in Vertisols, Dance Bayou, Brazoria County, Texas, U.S.A.: Implications for estimating paleoatmospheric PCO_2. *Journal of Sedimentary Research*, *81*(6), 394–400. https://doi.org/10.2110/jsr.2011.36

Mix, H. T., Mulch, A., Kent-Corson, M. L., & Chamberlain, C. P. (2011). Cenozoic migration of topography in the North American Cordillera. *Geology*, *39*(1), 87–90. https://doi.org/10.1130/G31450.1

Morrill, C., & Koch, P. L. (2002). Elevation or alteration? Evaluation of isotopic constraints on paleoaltitudes surrounding the Eocene Green River Basin. *Geology*, *2*, 151–154.

Nativ, R., & Riggio, R. (1990). Precipitation in the Southern High Plains: Meteorologic and isotopic features. *Journal of Geophysical Research*, *95*(D13), 22559. https://doi.org/10.1029/JD095iD13p22559

Nordt, L. C., Dworkin, S. I., & Atchley, S. C. (2011). Ecosystem response to soil biogeochemical behavior during the Late Cretaceous and early Paleocene within the western interior of North America. *Bulletin of the Geological Society of America*, *123*(9–10), 1745–1762. https://doi.org/10.1130/B30365.1

Pagani, M., Zachos, J. C., Freeman, K. H., Tipple, B. J., & Bohaty, S. M. (2005). Marked decline in atmospheric carbon dioxide concentrations during the Paleogene. *Science*, *309*(5734), 600–603. https://doi.org/10.1126/science.1110063

Passey, B. H., & Henkes, G. A. (2012). Carbonate clumped isotope bond reordering and geospeedometry. *Earth and Planetary Science Letters*, *351–352*, 223–236. https://doi.org/10.1016/j.epsl.2012.07.021

Passey, B. H., Levin, N. E., Cerling, T. E., Brown, F. H., & Eiler, J. M. (2010). High-temperature environments of human evolution in East Africa based on bond ordering in paleosol carbonates. *Proceedings of the National Academy of Sciences of the United States of America*, *107*(25), 11245–11249. https://doi.org/10.1073/pnas.1001824107

Pearson, P. N., Ditchfield, P. W., Singano, J., Harcourt-Brown, K. G., Nicholas, C. J., Olsson, R. K., et al. (2001). Warm tropical sea surface temperatures in the Late Cretaceous and Eocene epochs. *Nature*, *413*(6855), 481–487. https://doi.org/10.1038/35097000

Pearson, P. N., van Dongen, B. E., Nicholas, C. J., Pancost, R. D., Schouten, S., Singano, J. M., et al. (2007). Stable warm tropical climate through the Eocene epoch. *Geology*, *35*(3), 211–214. https://doi.org/10.1130/G23175A.1

Peters, N. A., Huntington, K. W., & Hoke, G. D. (2013). Hot or not? Impact of seasonally variable soil carbonate formation on paleotemperature and O-isotope records from clumped isotope thermometry. *Earth and Planetary Science Letters*, *361*, 208–218. https://doi.org/10.1016/j.epsl.2012.10.024

Philpotts, A. R. (1990). *Principles of igneous and metamorphic petrology*. Englewood Cliffs, NJ: Prentice Hall.

Pross, J., Contreras, L., Bijl, P. K., Greenwood, D. R., Bohaty, S. M., Schouten, S., et al. (2012). Persistent near–tropical warmth on the antarctic continent during the early Eocene epoch. *Nature*, *488*(7409), 73–77. https://doi.org/10.1038/nature11300

Quade, J., Eiler, J., Daëron, M., & Achyuthan, H. (2013). The clumped isotope geothermometer in soil and paleosol carbonate. *Geochimica et Cosmochimica Acta*, *105*, 92–107. https://doi.org/10.1016/j.gca.2012.11.031

Quade, J., Garzione, C., & Eiler, J. (2007). Paleoelevation reconstruction using pedogenic carbonates. *Reviews in Mineralogy and Geochemistry*, *66*(1), 53–87. https://doi.org/10.2138/rmg.2007.66.3

Quade, J., Rech, J. A., Latorre, C., Betancourt, J. L., Gleeson, E., & Kalin, M. T. K. (2007). Soils at the hyperarid margin: The isotopic composition of soil carbonate from the Atacama Desert, Northern Chile. *Geochimica et Cosmochimica Acta*, *71*(15), 3772–3795. https://doi.org/10.1016/j.gca.2007.02.016

Rapp, S. D., MacFadden, B. J., & Schiebout, J. A. (1983). Magnetic polarity stratigraphy of the Early Tertiary Black Peaks Formation, Big Bend National Park, Texas. *The Journal of Geology*, *91*(5), 555–572. https://doi.org/10.1086/628804

Ringham, M. C., Hoke, G. D., Huntington, K. W., & Aranibar, J. N. (2016). Influence of vegetation type and site-to-site variability on soil carbonate clumped isotope records, Andean piedmont of Central Argentina (32–34°S). *Earth and Planetary Science Letters*, *440*, 1–11. https://doi.org/10.1016/j.epsl.2016.02.003

Roberts, C. D., Legrande, A. N., & Tripati, A. K. (2009). Climate sensitivity to Arctic seaway restriction during the early Paleogene. *Earth and Planetary Science Letters*, *286*(3–4), 576–585. https://doi.org/10.1016/j.epsl.2009.07.026

Rohling, E. J., Sluijs, A., Dijkstra, H. A., Köhler, P., Van De Wal, R. S. W., Von Der Heydt, A. S., et al. (2012). Making sense of palaeoclimate sensitivity. *Nature*, *491*(7426), 683–691. https://doi.org/10.1038/nature11574

Rothstein, D., & Manning, C. (2003). Geothermal gradients in continental magmatic arcs: Constraints from the eastern Peninsular Ranges batholith, Baja California, México. *Geological Society of America, Special Paper*, 337–354.

Royer, D. L., Donnadieu, Y., Park, J., Kowalczyk, J., & Godderis, Y. (2014). Error analysis of CO_2 and O_2 estimates from the long-term geochemical model GEOCARBSULF. *American Journal of Science*, *314*(9), 1259–1283. 2014.01, DOI: https://doi.org/10.2475/09.2014.01

Royer, D. L., Osborne, C. P., & Beerling, D. J. (2002). High CO_2 increases the freezing sensitivity of plants: Implications for paleoclimatic reconstructions from fossil floras. *Geology*, *30*(11), 963–966. https://doi.org/10.1130/0091-7613(2002)030<0963

Rozanski, K., Araguás-Araguás, L., & Gonfiantini, R. (1993). Isotopic patterns in modern global precipitation. *Climate Change in Continental Isotopic Records*, 1–36. https://doi.org/10.1029/GM078p0001

Sagoo, N., Valdes, P. J., Flecker, R., & Gregoire, L. J. (2013). The early Eocene equable climate problem: Can perturbations of climate model parameters identify possible solutions? *Philosophical Transactions. Series A, Mathematical, Physical, and Engineering Sciences*, *371*(2001), 20130123. https://doi.org/10.1098/rsta.2013.0123

Santrock, J., Studley, A., & Hayes, J. M. (1985). Isotopic analyses based on the mass spectra of carbon dioxide. *Analytical Chemistry*, *57*(7), 1444–1448.

Schauer, A. J., Kelson, J., Saenger, C., & Huntington, K. W. (2016). Choice of ^{17}O correction affects clumped isotope (Δ_{47}) values of CO_2 measured with mass spectrometry. *Rapid Communications in Mass Spectrometry*, *30*(24), 2607–2616. https://doi.org/10.1002/rcm.7743

Schiebout, J. A., Rigsby, C. A., Rapp, S. D., Hartnell, J. A., & Standhardt, B. R. (1987). Stratigraphy of the cretaceous-tertiary and Paleocene-Eocene transition rocks of big bend National Park, Texas. *The Journal of Geology*, *95*(3), 359–375. https://doi.org/10.1086/629135

Schmidt, D. R. (2009). Stable isotope geochemistry of Upper Cretaceous and Paleocene strata in Big Bend National Park, Texas. *Dissertation*. Texas Tech University.

Schmitz, B., & Pujalte, V. (2007). Abrupt increase in seasonal extreme precipitation at the Paleocene-Eocene boundary. *Geology*, *35*(3), 215–218. https://doi.org/10.1130/G23261A.1

Schubert, B. A., Jahren, A. H., Eberle, J. J., Sternberg, L. S. L., & Eberth, D. A. (2012). A summertime rainy season in the Arctic forests of the Eocene. *Geology*, *40*(6), 523–526. https://doi.org/10.1130/G32856.1

Sewall, J. O., & Sloan, L. C. (2001). Equable paleogene climates: The result of a stable, positive Arctic Oscillation? *Geophysical Research Letters*, *28*(19), 3693–3695. https://doi.org/10.1029/2001GL013776

Sewall, J. O., & Sloan, L. C. (2006). Come a little bit closer: A high-resolution climate study of the early Paleogene Laramide foreland. *Geology*, *34*(2), 81–84. https://doi.org/10.1130/G22177.1

Sharman, G. R., Covault, J. A., Stockli, D. F., Wroblewski, A. F. J., & Bush, M. A. (2017). Early Cenozoic drainage reorganization of the United States Western Interior-Gulf of Mexico sediment routing system. *Geology*, *45*(2), 187–190. https://doi.org/10.1130/G38765.1

Shellito, C. J., Lamarque, J., & Sloan, L. C. (2009). Early Eocene Arctic climate sensitivity to pCO_2 and basin geography. *Geophysical Research Letters*, *36*, L09707. https://doi.org/10.1029/2009GL037248

Shellito, C. J., Sloan, L. C., & Huber, M. (2003). Climate model sensitivity to atmospheric CO_2 levels in the early-middle Paleogene. *Palaeogeography, Palaeoclimatology, Palaeoecology*, *193*(1), 113–123. https://doi.org/10.1016/S0031-0182(02)00718-6

Sherwood, S. C., & Huber, M. (2010). An adaptability limit to climate change due to heat stress. *Proceedings of the National Academy of Sciences*, *107*(21), 9552–9555. https://doi.org/10.1073/pnas.0913352107

Sloan, L. C. (1994). Equable climates during the early Eocene: significance of regional paleogeography for North American climate. *Geology*, *22*(10), 881–884. https://doi.org/10.1130/0091-7613(1994)022<0881:ECDTEE>2.3.CO

Sloan, L. C., & Barron, E. J. (1990). "Equable" climates during Earth history? *Geology*, *18*(6), 489–492. https://doi.org/10.1130/0091-7613(1990)018<0489:ECDEH>2.3.CO;2

Sluijs, A., Röhl, U., Schouten, S., Brumsack, H.-J., Sangiorgi, F., Damsté, J. S. S., et al. (2008). Arctic late Paleocene–early Eocene paleoenvironments with special emphasis on the Paleocene-Eocene thermal maximum (Lomonosov Ridge, Integrated Ocean Drilling Program Expedition 302). *Paleoceanography*, *23*, PA1S11. https://doi.org/10.1029/2007PA001495

Sluijs, A., Schouten, S., Donders, T. H., Schoon, P. L., Röhl, U., Reichart, G.-J., et al. (2009). Warm and wet conditions in the Arctic region during Eocene Thermal Maximum 2. *Nature Geoscience*, *2*(11), 777–780. https://doi.org/10.1038/ngeo668

Sluijs, A., Schouten, S., Pagani, M., Woltering, M., Brinkhuis, H., Damsté, J. S. S., et al. (2006). Subtropical Arctic Ocean temperatures during the Palaeocene/Eocene thermal maximum. *Nature*, *441*(7093), 610–613. https://doi.org/10.1038/nature04668

Smith, M. E., Carroll, A. R., Scott, J. J., & Singer, B. S. (2014). Early Eocene carbon isotope excursions and landscape destabilization at eccentricity minima: Green River Formation of Wyoming. *Earth and Planetary Science Letters*, *403*, 393–406. https://doi.org/10.1016/j.epsl.2014.06.024

Smith, R. Y., Basinger, J. F., & Greenwood, D. R. (2009). Depositional setting, fossil flora, and paleoenvironment of the early Eocene Falkland site, Okanagan Highlands, British Columbia. *Canadian Journal of Earth Sciences*, *46*(11), 811–822. https://doi.org/10.1139/E09-053

Snell, K. E., Thrasher, B. L., Eiler, J. M., Koch, P. L., Sloan, L. C., & Tabor, N. J. (2013). Hot summers in the Bighorn Basin during the early Paleogene. *Geology*, *41*(1), 55–58. https://doi.org/10.1130/G33567.1

Spicer, R. A., Herman, A. B., Liao, W., Spicer, T. E. V., Kodrul, T. M., Yang, J., et al. (2014). Cool tropics in the middle Eocene: Evidence from the Changchang Flora, Hainan Island, China. *Palaeogeography, Palaeoclimatology, Palaeoecology*, *412*, 1–16. https://doi.org/10.1016/j.palaeo.2014.07.011

Spicer, R. A., & Parrish, J. T. (1990). Late Cretaceous-early Tertiary palaeoclimates of northern high latitudes: A quantitative view. *Journal of the Geological Society*, *147*(2), 329–341. https://doi.org/10.1144/gsjgs.147.2.0329

Stolper, D. A., & Eiler, J. M. (2015). The kinetics of solid-state isotope-exchange reactions for clumped isotopes: A study of inorganic calcites and apatites from natural and experimental samples. *American Journal of Science*, *315*(5), 363–411. 2015.01. https://doi.org/10.2475/05.2015.01

Thomas, W., Ursula, R., Barbara, D., McCarren, K. H., & Zachos, C. J. (2011). A complete high-resolution Paleocene benthic stable isotope record for the Central Pacific (ODP site 1209). *Paleoceanography*, *26*, PA2216. https://doi.org/10.1029/2010PA002092

Thrasher, B. L., & Sloan, L. C. (2009). Carbon dioxide and the early Eocene climate of western North America. *Geology*, *37*(9), 807–810. https://doi.org/10.1130/G30090A.1

Thrasher, B. L., & Sloan, L. C. (2010). Land cover influences on the regional climate of western North America during the early Eocene. *Global and Planetary Change*, *72*(1–2), 25–31. https://doi.org/10.1016/j.gloplacha.2010.02.002

Tierney, J. E., Sinninghe Damsté, J. S., Pancost, R. D., Sluijs, A., & Zachos, J. C. (2017). Eocene temperature gradients. *Nature Geoscience*, *10*(8), 538–539. https://doi.org/10.1038/ngeo2997

Tindall, J., Flecker, R., Valdes, P., Schmidt, D. N., Markwick, P., & Harris, J. (2010). Modelling the oxygen isotope distribution of ancient seawater using a coupled ocean–atmosphere GCM: Implications for reconstructing early Eocene climate. *Earth and Planetary Science Letters*, *292*(3–4), 265–273. https://doi.org/10.1016/j.epsl.2009.12.049

Tripati, A. K., Delaney, M. L., Zachos, J. C., Anderson, L. D., Kelly, D. C., Elderfield, H., et al. (2003). Tropical sea-surface temperature reconstruction for the early Paleogene using Mg/Ca ratios of planktonic foraminifera. *Paleoceanography*, *18*(4), 1101. https://doi.org/10.1029/2003PA000937

Turcotte, D., & Schubert, G. (2014). *Geodynamics*. Cambridge, UK: Cambridge Univ. Press. https://doi.org/10.1017/CBO9780511843877

Turner, K. J., Berry, M. E., Page, W. R., Lehmann, T. M., Bohannon, R. G., Scott, R. B., et al. (2011). Geologic map of Big Bend National Park, Texas. U.S. Geological Survey Scientific Investigations Map 3142, 84.

Vachon, R. W., Welker, J. M., White, J. W. C., & Vaughn, B. H. (2010). Monthly precipitation isoscapes ($\delta^{18}O$) of the United States: Connections with surface temperatures, moisture source conditions, and air mass trajectories. *Journal of Geophysical Research*, *115*, D21126. https://doi.org/10.1029/2010JD014105

Valdes, P. (2011). Built for stability. *Nature Geoscience*, *4*(7), 414–416. https://doi.org/10.1038/ngeo1200

Valdes, P., Armstrong, E., Badger, M. P. S., Bradshaw, C. D., Bragg, F., Davies-Barnard, T., et al. (2017). The BRIDGE HadCM3 family of climate models: HadCM3@Bristol v1.0. *Geoscientific Model Development Discussion*, 1–42. https://doi.org/10.5194/gmd-2017-16

van Hinsbergen, D. J. J., de Groot, L. V., van Schaik, S. J., Spakman, W., Bijl, P. K., Sluijs, A., et al. (2015). A paleolatitude calculator for paleoclimate studies. *PLoS One*, *10*(6), e0126946. https://doi.org/10.1371/journal.pone.0126946

Vera, C., Higgins, W., Amador, J., Ambrizzi, T., Garreaud, R., Gochis, D., et al. (2006). Toward a unified view of the American monsoon systems. *American Meteorological Society*, *19*, 4977–5000.

Watford, D. (2015). An early Paleogene terrestrial paleoclimate record from Big Bend National Park, Texas; Insights from carbonate clumped isotope thermometry. The University of Utah, ProQuest Dissertations Publishing, 2015.10,011,603.

Weijers, J. W. H., Schouten, S., Sluijs, A., Brinkhuis, H., & Sinninghe Damsté, J. S. (2007). Warm arctic continents during the Palaeocene-Eocene thermal maximum. *Earth and Planetary Science Letters*, *261*(1–2), 230–238. https://doi.org/10.1016/j.epsl.2007.06.033

Wheeler, E. A. (1991). Paleocene dicotyledonous trees from big bend National Park, Texas: Variability in wood types common in the Late Cretaceous and Early Tertiary, and ecological inferences. *American Journal of Botany*, *78*(5), 658–671. https://doi.org/10.1002/j.1537-2197.1991.tb12590.x

Wheeler, E. A., & Lehman, T. M. (2005). Upper Cretaceous-Paleocene conifer woods from Big Bend National Park, Texas. *Palaeogeography, Palaeoclimatology, Palaeoecology*, *226*(3–4), 233–258. https://doi.org/10.1016/j.palaeo.2005.05.014

White, P. D., & Schiebout, J. (2008). Paleogene paleosols and changes in pedogenesis during the initial Eocene Thermal Maximum: Big Bend National Park, Texas, USA. *Bulletin of the Geological Society of America*, *120*(11–12), 1347–1361. https://doi.org/10.1130/B25987.1

Wing, S., & Greenwood, D. (1993). Fossils and fossil climate: The case for equable continental interiors in the Eocene. *Philosophical Transactions of the Royal Society of London B Biological Sciences*, *341*(1297), 243–252. https://doi.org/10.1098/rstb.1993.0109

Wing, S. L., Harrington, G. J., Smith, F. A., Bloch, J. I., Boyer, D. M., & Freeman, K. H. (2005). Transient floral change and rapid global warming at the Paleocene-Eocene boundary. *Science*, *310*, 993–996.

Wing, S. L., Herrera, F., Jaramillo, C. A., Gomez-Navarro, C., Wilf, P., & Labandeira, C. C. (2009). Late Paleocene fossils from the Cerrejon Formation, Colombia, are the earliest record of Neotropical rainforest. *Proceedings of the National Academy of Sciences*, *106*(44), 18,627–18,632. https://doi.org/10.1073/pnas.0905130106

Winguth, A., Shellito, C., Shields, C., & Winguth, C. (2010). Climate response at the Paleocene-Eocene thermal maximum to greenhouse gas forcing—A model study with CCSM3. *Journal of Climate*, *23*(10), 2562–2584. https://doi.org/10.1175/2009JCLI3113.1

Zachos, J. C., Dickens, G. R., & Zeebe, R. E. (2008). An Early Cenozoic perspective on greenhouse warming and carbon-cycle dynamics. *Nature*, *451*(7176), 279–283. https://doi.org/10.1038/nature06588

Zachos, J. C., Pagani, M., Sloan, L., Thomas, E., & Billups, K. (2001). Trends, global rhythms, aberrations in global climate 65 Ma to present. *Science*, *292*(5517), 686–693. https://doi.org/10.1126/science.1059412